UNIVERSITY OF OKLAHOMA

GRADUATE COLLEGE

AN EVALUATION OF CONSISTENCY FOR MULTIPLE REMOTELY SENSED DATA SOURCES

A THESIS

SUBMITTED TO THE GRADUATE FACULTY

In partial fulfillment of the requirements for the

Degree of

MASTER OF SCIENCE

By
Ethan James Heck
Norman, Oklahoma
2020

AN EVALUATION OF CONSISTENCY FOR MULTIPLE

REMOTELY SENSED DATA SOURCES

A THESIS APPROVED FOR THE
DEPARTMENT OF GEOGRAPHY AND ENVIRONMENTAL SUSTAINABILITY

BY THE COMMITTEE CONSISTING OF

_____

Dr. Kirsten de Beurs, Chair

_____

Dr. Jennifer Koch

_____

Dr. Mike Wimberly

Acknowledgements

I would first like to thank my advisor, Dr. Kirsten de Beurs, for her support beginning as an undergraduate student until the completion of my master's. I will always be grateful for her guidance and investment in my education. This journey has been advantageous for me professionally as well as personally, and it would not have been possible without her motivation and belief in me.

I would also like to extend my sincere thanks to the rest of my committee members Dr. Jennifer Koch and Dr. Mike Wimberly. Your questions and support have improved my research, and I am genuinely thankful for the time you have invested. Additionally, I would like to acknowledge Braden Owsley and Geoff Henebry for their contributions to the work presented in Chapter 2.

Finally, I would like to thank my wife and parents for their unwavering support. Collectively, each of them has played many roles, such as a motivational speaker, counselor, and last but not least, financial support. This journey would not have been completed without their sacrifice and encouragement.

Table of Contents

List of Tables

List of Figures

Abstract

Archive continuation through succeeding satellite missions is highly important in preserving and creating deep repositories of information for Earth observation. However, with varying spectral and spatial resolution, it can be a challenge to harmoniously continue archives through different platforms such as planned with MODIS and VIIRS. I first evaluate the consistency between two collections of the Moderate Resolution Imaging Spectroradiometer (MODIS) data to highlight discrepancies that can exist between dataset even when the data is collected from the same sensor. Three different MODIS products are investigated to determine the extent that improvements made to C6 influence the overall trend results for time series between 2001 and 2017. I focus on these three products specifically, both to allow for a comparison of vegetation index products—NDVI (Normalized Difference Vegetation Index) and EVI (Enhanced Vegetation Index) from MOD13C1, and NDVI and EVI calculated based on surface reflectance from MCD43C4—and also to gain an understanding of the improvements on an entirely different product from the same sensor, namely Land Surface Temperature (LST) from MOD11C2. Next, I evaluate the consistency of MODIS and the Visible Infrared Imaging Radiometer Suite (VIIRS) to contribute to the knowledge of how seamlessly VIIRS can be used in the continuation of the MODIS archive. The MYD09GA and MCD43A4 products from MODIS, as well as the VNP09GA and VNP43IA4 products from VIIRS are used to carry out the analysis. In addition to surface reflectance, I also evaluate NDVI and the tasseled cap transformations of brightness, greenness, and wetness. I have conducted this analysis on the north island of New Zealand because the multiple land covers and their fragmented tendencies are a very good representation of how well the sensors correlate in potentially complex land surface scenarios.

Chapter 1: Introduction

Remotely sensed data is the only feasibly means to monitor regional to large scale change of the terrestrial land surface. Whether we seek to answer questions temporally about phenological processes or multi-decadal change, continued archives of data collected from satellites will be depended on by the scientific community. There are several remotely sensed data sources that are cost free for end users, each of which offer varying spatial, spectral, temporal, and radiometric resolutions. A source such as the Moderate Resolution Imaging Spectroradiometer (MODIS) aboard the Terra and Aqua satellites provides data products at a high temporal (daily) resolution but comes at the cost of a relatively coarse spatial resolution, providing products at 250, 500, 1000, and 5600 meters. Similarly, the Visible Infrared Imaging Radiometer Suite (VIIRS) is a sensor that is equipped on the National Polar-orbiting Partnership (NPP) satellite. VIIRS shares a similar temporal/spatial resolution trade-off and offers MODIS-like products in an effort to create archive continuity. Conversely, the Landsat missions provide a moderately high spatial resolution of 30 meters but only has a temporal revisit time of ~16 days. An alternative but complimentary source to Landsat is the Sentinel-2 MultiSpectral Instrument (MSI) that offers a revisit time of about five days and has a spatial resolution of 10 – 20 meters for bands in the visible and near infrared portion of the electromagnetic spectrum.

Vegetation indices (VI) are widely used and one of the oldest tools used in remote sensing studies. There are several variations, but most are built around the ratio of reflected light in the red and near infrared (NIR) spectrum (Glenn et al., 2008). The most widely used is the Normalized Difference Vegetation Index (NDVI) (Tucker, 1979):

$$\text{NDVI} = (\text{NIR} - \text{Red})/(\text{NIR} + \text{Red})$$

The NDVI normalizes values between -1 to 1 with dense vegetation having high positive values, while bare ground will be low positive values and water will display negative values because of the absorption in the NIR (Glenn et al., 2008).

The Enhanced Vegetation Index is also widely used and is calculated with the red, NIR, blue and corresponding coefficients.

$$\text{EVI} = 2.5(\text{NIR} - \text{Red})/(1 + \text{NIR} + (\ (6)\ \text{Red} - (7.5)(\text{Blue}))$$

the coefficient of 1 accounts for canopy background scattering while the red and blue coefficients of 6 and 7.5, minimize aerosol variations (Glenn et al., 2008). The EVI in comparison to the NDVI is less prone to saturation in densely vegetated areas.

AVHRR aboard NOAA's Polar Orbiting Environmental Satellites (POES) established a coarse resolution archive of data about the terrestrial surface. The long-term record established by AVHRR has been continued by MODIS, primarily through the NDVI. In addition to the continued NDVI record, MODIS has contributed an extensive repository of 20+ years of data products that include VI, surface reflectance, albedo, and land surface temperature (LST). MODIS is collected by two MODIS sensors aboard the Terra and Aqua satellites that have been in service since 1999 and 2002, respectively.

After 20 years of reliable service from MODIS, now comes a time where the scientific communities that have relied on the archives must become interested in the succeeding sensor to MODIS. VIIRS has been designed for continuity of MODIS through the creation of MODIS like products using similar collection methods and algorithms. Although VIIRS and MODIS have significant differences, the spatial, spectral, and temporal similarities potentially could allow for a continued archive.

I will explore data continuity in this thesis. First, I evaluate VI and LST trends throughout a 16-year time series from MODIS collections 5 and 6. The MODIS collections are reprocessed

versions of the MODIS archive that have algorithm adjustments for improved accuracy and correction for the degradation of sensors. Although the data are from the same sensors and products, we see that the reprocessing of data provides significantly different results. Next, I expand this idea and investigate the comparability of data products from different sensors. I evaluate the correlation between MODIS, VIIRS and Landsat across four land cover types in New Zealand. I first explore the similarities of MODIS with VIIRS to evaluate how seamlessly the datasets compare by land cover type due to VIIRS being the designated successor.

The continued archive of MODIS is characterized by the periodic roll out of new collections that apply improvements to the archive. These improvements are in the form of algorithm improvements or calibration adjustments that improve product accuracy or adjust for the negative impacts of sensor degradation. At the time of writing, the most current collection is collection 6, and in this study, I evaluate the significant differences between the most recent collection and the previous, collection 5. The significant differences are evaluated through the Seasonal Kendall trend test on the NDVI, EVI, and LST. Through evaluating the VI and LST, I demonstrate that there are significant differences between the two collections, primarily in the VI. These findings bring to light that studies which currently use or that have previously used MODIS data should reconsider results based on the collection of MODIS data that was applied to the analysis. Even within the same data stream, there can be significant differences based on algorithm changes and calibrations adjustments even when the spatial, temporal, spectral, and radiometric resolutions remained constant. Therefore, since we see that data can be significantly different by the same sensor, I search to evaluate how well MODIS and VIIRS correlate, as VIIRS is the designed successor of MODIS.

The MODIS archive has even built on the previously established NDVI record of AVHRR, as the two data streams have proved to be comparable with minor adjustments. MODIS

has continued to be an important data source in many scientific communities, even now, operating well past its design life. The years of service for MODIS and the noticeable degradation to the Terra sensor (Lyapustin et al., 2014; Heck et al., 2019), should prompt users to start exploring data streams that can replace or extend the long-standing MODIS archive. VIIRS was designed with similar parameters, and the data products are processed to be similar to the ones provided by MODIS. However, there are differences between the two sensors that can have a negative impact on the correlation of the data. Although MODIS and VIIRS have varying specifications, the continued NDVI record established by AVHRR and continued through MODIS serves as a successful case study for multi-sensor continued archives.

MODIS and AVHRR vary in red and NIR bandwidth and compositing techniques. Maximum value composites are typically used for AVHRR where the greatest NDVI value observed for each pixel is selected for each 16-day composite. MODIS data are typically processed using a constrained-view angle-maximum value composite where the two greatest observed values per pixel are selected and the composite is finalized using the nearest to nadir observation (Gallo et al., 2004). The NDVI averages from these two sensors across all land cover types were similar, the AVHRR average was 0.389 (standard deviation of 0.223) while the average MODIS NDVI was 0.423 (standard deviation of 0.247). In any comparison of different platforms, discordance should be expected from varying resolution, degradation, equatorial crossing time, or satellite drift. Although there is a slight variation in NDVI averages, the two sensors showed seasonal similarity and were quite similar when sampled over coinciding time intervals, spatial areas and land cover types (Gallo et al., 2004). AVHRR and MODIS are an example of multi-sensor archive continuation under similar conditions, while comparable quality assurance processing such as cloud identification and water vapor corrections are performed on AVHRR (Gallo et al., 2005). Others have shown that that the correlation between the MODIS

and AVHRR NDVI datasets was high but displayed systematic and unsystematic differences (Ji et al. 2008). However, the systematic difference can be remedied by the application of a regression function to either dataset (Ji et al., 2008).

Therefore, we know that it reasonable to transition between platforms given the results presented, and others discussed later that have evaluated the relationship between MODIS and VIIRS. However, I demonstrate in this thesis that land cover can affect the results of the correlation, particularly when comparing forests and grasslands. Forests yield lower R^2 values in comparison to grasslands likely due to a more complex physical structure and a tendency to have cluster of data points rather than a linear relationship. Land cover type should be considered when pairing or transitioning between datasets and depending on application, adjustment may be required.

My thesis aims to show that careful attention should be given to data sources when implementing or reviewing research. Once we are aware of data inconsistencies, such as those discussed in chapter two between MODIS collection 5 & 6, it might be necessary to re-evaluate results using the revised version depending on spatial location and land cover type. Further, I will contribute to the understanding and outlook of multi-sensor archive continuation. MODIS has been in service for 20+ years and it will be imperative for many disciplines to understand its correlation with VIIRS.

Chapter 2: Evaluation of the MODIS Collections 5 and 6 for Change Analysis of Vegetation and Land Surface Temperature Dynamics in North and South America

This chapter was published with the following citation:

Heck E, de Beurs KM, Owsley BC, Henebry GM, 2019. Evaluation of the MODIS collections 5 and 6 for change analysis of vegetation and land surface temperature dynamics in North and South America. ISPRS Journal of Photogrammetry and Remote Sensing, 156 (121-134).

Abstract

The latest collection (C6) of MODIS data provides several algorithmic improvements and calibration adjustments that correct for sensor degradation, theoretically making the C6 MODIS products more accurate compared to previous collections. C6 adjustments also introduce several improvements in the vegetation index (VI) retrieval algorithms. With these improvements, we expect only minor differences between data from Terra and Aqua, but significantly different results between C5 and C6. In this paper, we investigate three different MODIS products to determine the extent that improvements made to C6 influence the overall trend results for time series between 2001 and 2017. We focus on these three products specifically, both to allow for a comparison of vegetation index products—NDVI and EVI from MOD13C1, and NDVI and EVI calculated based on surface reflectance from MCD43C4—and also to gain an understanding of the improvements on an entirely different product from the same sensor, namely Land Surface Temperature (LST) from MOD11C2. For the MCD43C4 dataset, we find that 17.9% and 16.4% of EVI and NDVI pixels, respectively, display trend discordance between C5 and C6. For the

MOD13C1 vegetation indices, we found comparable rates of trend discordance between C5 and C6: 18.5% and 17.4% for the EVI and NDVI pixels, respectively. For both products the greatest changes between C5 and C6 are an overall increase in pixels exhibiting a significant greening trend and an overall decline in pixels exhibiting a significant browning trend. Moreover, the largest differences between C5 and C6 for the NDVI and EVI data appear in cropland areas and in regions with relatively little human influence. In the Land Surface Temperature product (MOD11C2), the discordance between C5 and C6 is much lower: only 3.2% of day and 5.0% of night LST trends exhibited discordance between C5 and C6. We analyze the complementary results of vegetation index and land surface temperature trends and demonstrate that combining the results from different products observed at different portions of the electromagnetic spectrum—but linked through the biogeophysical processes of surface energy balance—allows us to portray change with more confidence than when relying on vegetation index data alone.

Keywords: change analysis, western hemisphere, NDVI, EVI, LST

1. Introduction

Satellites provide the ability to observe large spatial areas over long periods, enabling researchers the opportunity to reveal both abrupt and subtle changes in the vegetated land surface (de Beurs *et al.*, 2015, de Beurs *et al.*, 2018, Fan and Liu, 2016). To allow such analysis, it is important to carefully analyze and compare image time series so that the behaviors of the sensors and the algorithms that generate products can be well understood. With a better understanding of our data sources, researchers can be more confident that no false changes or trends are being reported, for example, due to operational error or degradation of the sensors (Wang *et al.*, 2012, Zhang & Roy, 2016). There is now an abundance of freely available data from multiple remote sensing platforms, enabling comparative studies to analyze the consistency and accuracy of these data. It is important to assess the stability across sensor platforms to create long standing archives (Fan & Liu, 2016) but as operational life rises (Belward & Skoien, 2015) it will become increasingly essential to understand how degradation over time impacts results and how degradation can be separated from other observed changes. The Moderate Resolution Imaging Spectroradiometer (MODIS), launched first onboard the Terra spacecraft in December 1999 and later onboard Aqua in May 2002, forms the basis for several clearly documented and freely available products at various spatial and temporal resolutions. The periodically renewed product "collections", which result from algorithmic adjustments and improvements, provide strong argument for using the MODIS products.

Over the years several improvements have been made to the MODIS products from one collection to the next. After changes are approved for each new collection, the entire MODIS archive is reprocessed to ensure that users have access to the most consistent and accurate data possible. The latest MODIS collection (C6) provides several algorithm improvements and calibration adjustments that correct for sensor degradation, theoretically making the products more

accurate. For example, one important aspect that affects all products based on MODIS Terra data is the correction for sensor degradation. There has been noticeable degradation in both the Terra and Aqua MODIS sensors, but previous research has shown there was substantially greater impact on the Terra sensor (Lyapustin *et al.*, 2014). The sensors are launched with onboard equipment, such as a solar diffuser and a solar diffuser stability monitor to perform periodic calibration, but this equipment can also experience operational degradation (Wang *et al.*, 2012, Xiong *et al.*, 2001). Two documented events are reported to have had significant impact on Terra's degradation. First, during a pre-launch thermal vacuum test, a portion of the door paint came off the nadir aperture door and coated parts of the optics and scanning mirror. The paint was cleaned but lasting residue or damage to protective coating appears to have impacted performance (Lyapustin *et al.*, 2014). Second, in May 2003, the solar door was permanently opened, and the solar door screen closed. The fixed position of this equipment has caused the solar door plate to degrade at a quicker rate, decreasing the reflectivity (Lyapustin *et al.*, 2014). The implication of decreasing reflectivity is a reduced capability to track sensor response over time (Lyapustin *et al.*, 2014). These events lead us to expect significant differences between the data collected from the MODIS sensors aboard Terra and Aqua.

The collection 6 adjustments were implemented not only to correct sensor degradation impacts, but also to introduce several improvements in the vegetation index (VI) retrieval algorithms (Didan *et al.* 2015). With these improvements, we expect only minor differences between the Terra and Aqua products, but significantly different results between C5 and C6 (Zhang *et al.*, 2017). Other papers have explored the differences between trends in VI data based on collections 5 and 6. For example, Detsch et al (2016) applied the Seasonal Kendall trend test to compare Terra and Aqua MODIS VI data from C5 and C6 for the period 2003-2010 in a study area surrounding the Kilimanjaro region of Tanzania. They found that at a seasonal scale, products created from Terra

and Aqua in C5 and C6 compared well with each other. However, throughout the length of the time series, the negative impacts created by the degradation of MODIS Terra were noticeable; the NDVI collected from Terra in C5 displayed more browning and less intense greening in comparison to the NDVI product collected from Aqua. The NDVI collected from Terra in C6 now displays more greening compared to the Aqua product. The presence of more greening trends in collection 6 points to the calibration changes that were made to compensate for degradation in the Terra MODIS.

A global comparison of collection 5 and 6 VIs focused only on trends in the annual maximum vegetation index (Zhang *et al.*, 2017). They noted sensor degradation in both Terra and Aqua: during the time span of 2003-2015, Aqua experienced an increase in NDVI of 0.03% $year^{-1}$ and an increase in EVI of 0.11% $year^{-1}$ from C5 to C6, respectively. We also expect to find at least some minor differences in MODIS land surface temperature data (LST) between C5 and C6, but there are few comparative studies covering the LST products.

In our analysis, we investigate four MODIS products (MOD13C1, MCD43C4, MCD43A4 and MOD11C2) to determine the extent that changes made to C6 impact the overall trend results. We compare vegetation index products—the NDVI and EVI available from MOD13C1 with the NDVI and EVI calculated from MCD43C4 and MCD43A4. We also explore changes in LST from MOD11C2 to see if the changes in trends evident in the VIs are also apparent in a different product from the same sensor. Our study differs from previous studies (Detsch *et al.*, 2016, Zhang *et al.*, 2017) in that we focus less on the difference between Terra and Aqua and more on the comparison between C5 and C6. We also apply a nonparametric trend analysis that is less sensitive than simple linear regression to outliers, seasonality, and autocorrelation (de Beurs & Henebry, 2004). Unlike many related studies, we look beyond the regional scale and calculate the trend results for the entire Western Hemisphere (excluding Greenland because of its extensive ice cover). We have

previously demonstrated that the use of more than a single index time series can significantly improve trend interpretation and attribution, and we have advocated for the use of complementary suites of multiple indicators as the new standard approach for change analysis (de Beurs *et al.*, 2015). Here we will follow this approach and not only investigate the changes in the vegetation indices by themselves, but also link the vegetation changes with warming and cooling of the land surface as observed by the land surface temperature data. Combining the results from different products observed at different regions of the electromagnetic spectrum—but linked through the biogeophysical processes of surface energy balance—allows us to portray change with more confidence than when relying on vegetation index data alone.

2. Data and Methods

2.1 C5 and C6 data for comparison

The focus of this study relies on trend results derived from vegetation index data (VI) and land surface temperature data (LST). VIs are spectral transformations of two or more bands designed to enhance the contribution of vegetation properties. Although many vegetation indices exist, two of the most widely used are the Normalized Difference Vegetation Index (NDVI) and the Enhanced Vegetation Index (EVI), and these are the primary datasets analyzed in this study.

We use four different products provided by MODIS, some collected from the Terra sensor alone (product name beginning with MOD) and another derived from a combination of both the Terra and Aqua MODIS sensors (product name beginning with MCD). The products have reached a stage three validation (Didan *et al.*, 2015, Schaaf, 2018), except for the LST product, which has achieved a stage two validation (Wan, 2014).

Both the MOD13 and the MCD43 products rely on MOD09GA and MYD09GA data, which are clear sky, multi-angle, high quality, atmospherically corrected, surface reflectance

products (Wang *et al.*, 2018). These two products use the M{O|Y}D09 data in slightly different ways. We outline in table S1 the salient improvements to collection 6 for the different data products.

We first evaluated the products at the Climate Modeling Grid (CMG) resolution (0.05°) to focus the analysis on the larger climate-driven results as opposed to changes as a result of human impacts, which are more easily visible in higher resolution data (de Beurs *et al.*, 2009). We then compared the trends in products at 500 m resolution for the VIs in four regions with substantial areas of trend disagreement between collections. All the data products were downloaded as global datasets for both C5 and C6. We applied the same processing methods to each dataset and present the results for North and South America, excluding Greenland. (Although the Amazon forest region is included in this study, extensive cloud cover generally limited data retrieval of sufficient quality to detect significant trends.) The NDVI and EVI were calculated from the MCD43 data, and all of the products were stacked to form time series. Quality assessment (QA) bands were used during this process to ensure that bad data (missing, clouds, snow/ice, *etc.*) did not corrupt the trend results, and that pixels with a high percentage of missing values (>70%) were filtered out in the final trend results.

2.1.1 MCD43C4 and MCD43A4 NBAR (Nadir BRDF- [Bidirectional Reflectance Distribution Function] Adjusted Reflectance) Data

These products provide NBAR for MODIS bands 1-7, which span the visible, near infrared, and shortwave infrared regions. In C5, NBAR data are delivered every 8 days using 16 days of observations, but in C6 they are delivered daily, still using 16 days of observations. The ninth day of collection is the listed day of year for the composite. For C6, we selected an observation every 8 days to correspond with the 8-day time series available for C5. The surface reflectance data are

corrected to a common nadir viewing geometry at the local solar noon zenith angle. The adjusted surface reflectance provides a good platform for vegetation index calculations and land cover classifications, and the product has achieved stage 3 validation.

2.1.2 MOD13C1 Vegetation Indices

This product is a 16-day composite that provides both the NDVI and the EVI. These VIs have been aggregated from the MOD13A2 (1 km) product and were projected to the CMG with a spatial resolution of 0.05° (~5.6 km). This product achieved stage 3 validation (Didan *et al.*, 2015). Notable improvements between C5 and C6 can be found in Table S1.

2.1.3 MOD11C2 Land Surface Temperature

This product is an 8-day composite of land surface temperature (LST) that provides daytime and nighttime LST in Kelvin at 0.05° spatial resolution. It has achieved stage 2 validation (Wan, 2008).

2.2 Ancillary data

We separate our trend results by land cover class, latitude, and anthropogenic influence.

2.2.1 MCD12C1 Yearly Land Cover Type

We used the MODIS land cover data with a spatial resolution of 0.05° (Sulla-Menashe & Friedl, 2018) and selected the International Geosphere-Biosphere Programme (IGBP) classification scheme for the most recent year available (2016). We selected the five largest land cover classes along with Croplands and Urban/Built-up lands for analysis of trend patterns (Table 1).

Table 1: Selected Land Cover Classes

Class	Description
Grasslands	Dominated by herbaceous annuals (<2m)
Savannas	Tree cover 10-30% (canopy >2m)
Evergreen Broadleaf Forests	Dominated by evergreen broadleaf and palmate trees (canopy >2m and tree cover > 60%),
Woody Savannas	Tree cover 30-60% (Canopy >2m)
Open Shrublands	Dominated by woody perennials (1-2m height and 10-60% cover)
Croplands	At least 60% of area is cultivated cropland
Urban/Built-up Lands	At least 30% impervious surface area including building materials, asphalt, and vehicles

2.2.2 Global Human Influence Index

The Human Influence Index (HII) is provided by NASA's Socioeconomic Data and Applications Center (SEDAC) and provides metric on human-environment interactions (Wildlife Conservation Society - WCS & Center for International Earth Science Information Network - CIESIN - Columbia University, 2005). The HII is a dataset with 1 km spatial resolution derived from nine global data layers that include population density, built-up areas, nighttime lights, land use, land cover, coastlines, roads, railroads, and navigable rivers. The range of values in the HII is 1-64, with 64 representing the greatest degree of human influence (Figure 1). We aggregated the most recent version of this dataset (2004) to match the trend results at 0.05° spatial resolution.

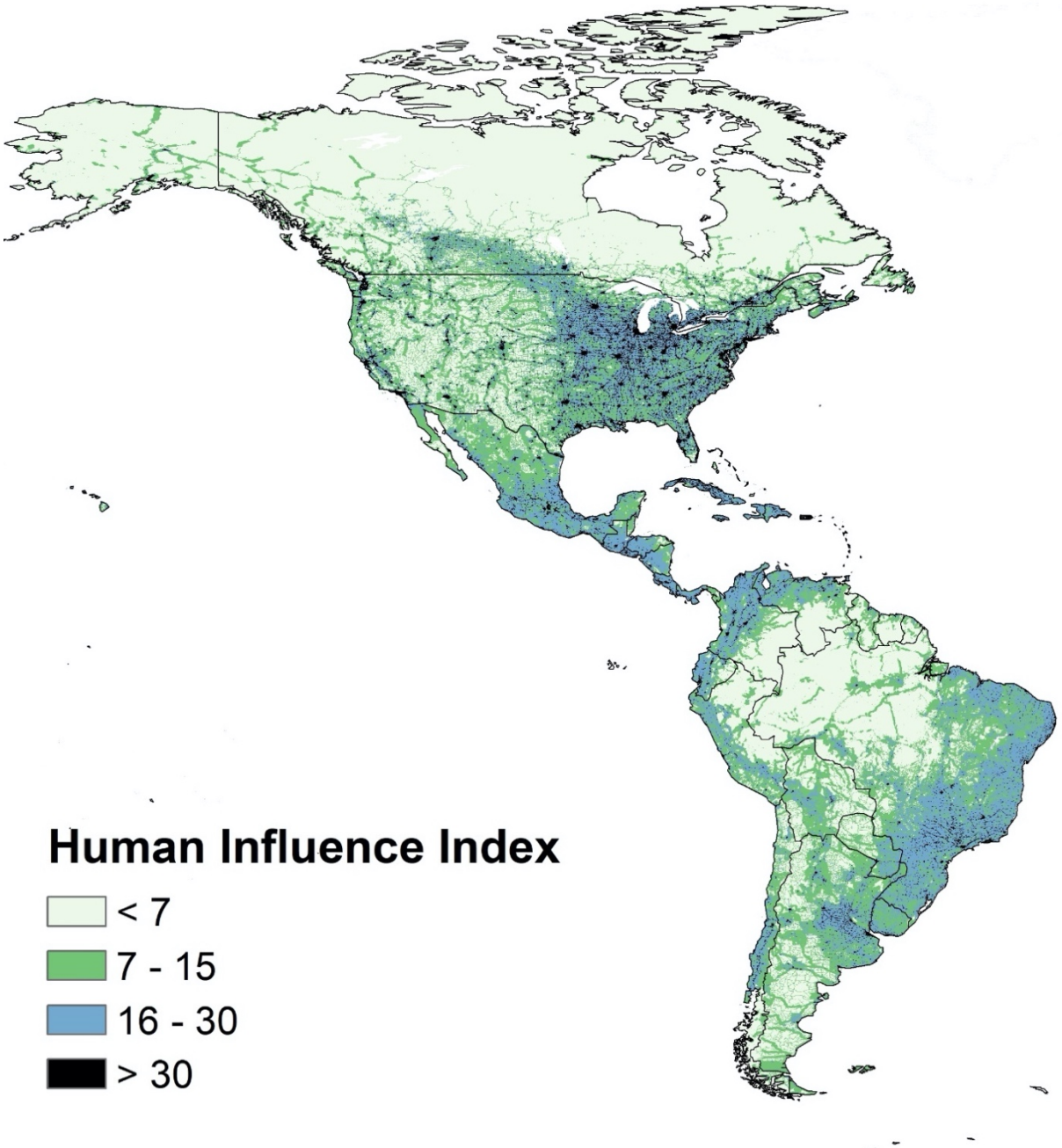

Figure 1: Human Influence Index (HII) throughout our study area. The HII has values that range from 1-64, with 64 representing the greatest human influence

2.3 Trend detection

We applied the Seasonal Kendall trend analysis to all C5 and C6 time series (MOD13C1, MCD43C4 and MOD11C2). The Seasonal Kendall trend test is completely rank based and robust against non-normality, missing values, seasonality, and corrected for first-order autocorrelation (de Beurs & Henebry, 2004). The Seasonal Kendall test is a variation of the Mann–Kendall test, where a separate Mann–Kendall test is run on each season. It tests for monotonic trends over the time series, yielding three possible results: positive trend, negative trend, or no trend. For the VIs, a positive trend corresponds to "greening" and a negative trend corresponds to "browning". For the LSTs, a positive trend corresponds to "warming" and a negative trend corresponding to "cooling". Furthermore, to ensure that meaningful trends are detected over the time series and to minimize spurious results, we selected a very conservative p-value ($p < 0.01$). After calculating the trend, we classify each grid cell as "no trend", "negative" (significantly decreasing trend), or "positive" (significantly increasing trend). Comparison of the maps of C5 and C6 trends create a difference map describing nine distinct outcomes (Table 2). These maps allow us to determine whether the trend patterns are consistent across both collections for the different products.

Table 2: Nine potential trend comparison outcomes

		C6		
		Negative trend	No trend	Positive trend
C5	Negative trend	**Concordance**	*Discordance*	***Extreme discordance***
	No trend	*Discordance*	**Concordance**	*Discordance*
	Positive trend	***Extreme discordance***	*Discordance*	**Concordance**

3. Results

An overview of all general trends for all products can be found in Table 3. We will discuss the differences in the individual products and the different collections below.

Table 3: Overview of trend results (% of all pixels) for all products.

	Negative		*Positive*		*No Trend*		*Missing*
Vegetation Index	**C5**	**C6**	**C5**	**C6**	**C5**	**C6**	**C5 and C6**
MCD43C4 EVI	9.52	3.83	3.27	14.56	65.07	59.47	22.13
MCD43C4 NDVI	7.76	4.35	3.95	15.38	66.14	58.12	22.14
MOD13C1 EVI	13.53	2.39	4.33	10.19	70.18	75.48	11.95
MOD13C1 NDVI	11.89	3.77	7.79	13.99	68.49	70.41	11.84
Land Surface Temperature							
MOD11C2 Day	0.78	1.07	3.90	3.60	83.12	83.13	12.20
MOD11C2 Night	0.02	0.04	6.02	4.51	76.85	78.34	17.11

3.1 MCD43C4

In Table 4 and Figure 2, we see that the NBAR VI trend results are missing for 22% of the pixels. Missing trend results occur where there are not enough time series values to produce a reliable trend. These areas are mainly in the Amazon Basin and Canadian Tundra, most likely a result of persistent cloud cover. Trend concordance (agreement between C5 and C6) occurs for 60% and 62% of the pixels for the EVI and NDVI, respectively. However, 17.9% and 16.4% of the EVI and NDVI pixels, respectively, exhibit trend discordance (disagreement between C5 and C6). The most frequent type of discordance occurs when no trend is evident in C5 but a significant positive (greening) trend appears in C6 (green in Figure 2; ~11% of pixels). The rarest outcomes were those of complete reversal, where the trend discordance is either the shift from positive in C5 to negative in C6 (blue in Figure 2) or the shift from negative in C5 to positive in C6 (red in Figure 2). The occurrence of these extreme trend discordances in the Western Hemisphere never exceeded 0.25%, and are all but invisible in Figure 2 except for the northern part of Chile, which is a hyper-arid desert. This part of the world is extremely dry with very limited vegetation, except for the occasional blooms (Chavez et al. 2019). It might not be surprising that it is in this setting that the

datasets reveal significantly different results, considering that the tested vegetation indices are not developed to monitor hyper-arid environments. For both the EVI and NDVI, we see fewer pixels with negative trends, more pixels with "no trends", and many more pixels with positive trends (Table 4). EVI and NDVI reveal similar discrepancies across the two collections.

We also evaluated the percentage of pixels with a significant trend in each dataset by latitude (Figure 2). The latitude graph presents the total percentage of positive or negative trends for the available pixels in each 5° latitudinal band; missing pixels are excluded from the percentage calculation. In Figure 2, for example, the positive EVI trends for C6 reveal two peaks of significant trend values, around 15°S and 20°N (darker green). Similar peaks are visible for C5, but the total percentage of area with a positive trend is much lower for C5. We show higher peaks in the negative trends for C5 (light purple) than for C6 (dark purple). The percentage of negative trends in C6 is limited with only a small peak around 20% at 40°S.

Table 4: MCD43C4 trend comparison results (% of all pixels) between C5 and C6 for both EVI and NDVI

MCD43C4 EVI	**C6**			**Missing data = 22.13**
C5	*Negative*	*No Trend*	*Positive*	*Total*
Negative	3.28	5.99	0.25	9.52
No Trend	0.55	53.46	11.06	65.07
Positive	<0.01	0.02	3.25	3.27
Total	3.83	59.47	14.56	Concordance = 59.99
MCD43C4 NDVI	**C6**			**Missing data = 22.14**
C5	*Negative*	*No Trend*	*Positive*	*Total*
Negative	3.64	4.04	0.08	7.76
No Trend	0.71	54.01	11.42	66.14
Positive	<0.01	0.07	3.88	3.95
Total	4.35	58.12	15.38	Concordance = 61.53

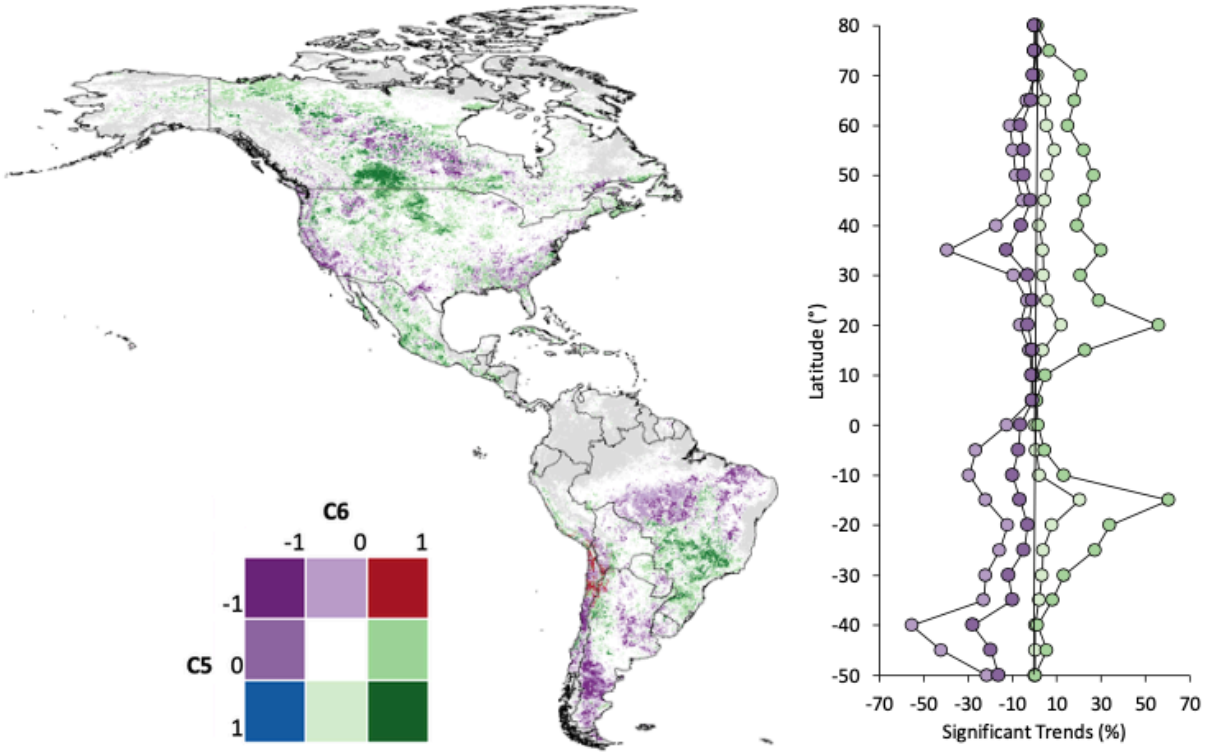

Figure 2: Comparison of MCD43C4 EVI C5 and C6. Nine different scenarios are presented. The greatest areas of discordance are no trends in C5 and positive in C6 (medium green), but there are also several areas that show no trends in C5 and negative trends in C6 (medium purple). Grey areas have insufficient data to support trend detection. NDVI results are very similar (not shown). The main discordant trends can be found in northern Chile where there are negative trends in C5 but positive trends in C6. The latitude graph reveals the total percentage of positive and negative trends in C5 (light purple and light green) and C6 (dark purple and dark green). Note that the trends in the latitude graph are not stacked.

3.2 MOD13C1

In Table 5 and corresponding Figure 3, we see that the concordances between collections in the EVI and NDVI are 69.6% and 70.8%, respectively. Compared to the MCD43C4 data, the percentage of missing values is lower and comparable at 11.95% for the EVI and 11.84% or the NDVI. It is important to realize that since we use an 8-day time series for the MCD43C4 data, and a 16-day time series for the MOD13C1 data, we have twice the probability of finding a missing value in the MCD43C4 dataset. The trend discordances between C5 and C6 are 18.5% and 17.4%

of the EVI and NDVI pixels, respectively, which is comparable to the MCD43C4 results. The percentages vary for each VI, but the overall patterns are consistent between the collections. For EVI, we find negative trends for 13.5% of the land area in C5, but just 2.4% in C6. While the total amount of negative trends decreases from C5 to C6, the positive EVI trends more than double between collections increasing from 4.3% in C5 to 10.1% in C6, and pixels with no significant trend ($p>0.01$) increases from 70.2% to 75.5%. There is relatively high trend concordance between NDVI and EVI for all but two outcomes (Table 5). We find that 11% of EVI pixels and 8% of NDVI pixels that display a negative trend in C5, exhibit no trend in C6. Similarly, there is a substantial shift of pixels from no trend in C5 to positive trend in C6 of 6.5% and 7.5% for the EVI and NDVI, respectively (Table 5). No pixels with positive trends in C5 appear with negative trends in C6.

The MOD13 data reveals similar peaks by latitude, but interestingly, the southern hemisphere positive peak appears around 20°S and, in the northern hemisphere, there is a positive peak around 25°N and another around 50°N. Both datasets reveal much higher peaks of positive trends in C6 than in C5. On the other hand, there are higher peaks of negative trends in C5 than in C6. The percentage of negative trends in C6 is limited with only a small peak around 20% at 40°S.

Table 5: MOD13C1 trend comparison results (% of all pixels) between C5 and C6 for both EVI and NDVI

MOD13C1 EVI	**C6**			**Missing data = 11.95**
C5	*Negative*	*No Trend*	*Positive*	*Total*
Negative	2.31	11.18	0.04	13.53
No Trend	0.08	63.62	6.48	70.18
Positive	0.00	0.66	3.67	4.33
Total	2.39	75.46	10.19	Concordance = 69.60
MOD13C1 NDVI	**C6**			**Missing data = 11.84**
C5	*Negative*	*No Trend*	*Positive*	*Total*
Negative	3.57	8.19	0.13	11.89
No Trend	0.20	60.83	7.46	68.49
Positive	0.00	1.39	6.40	7.79
Total	3.77	70.41	13.99	Concordance = 70.80

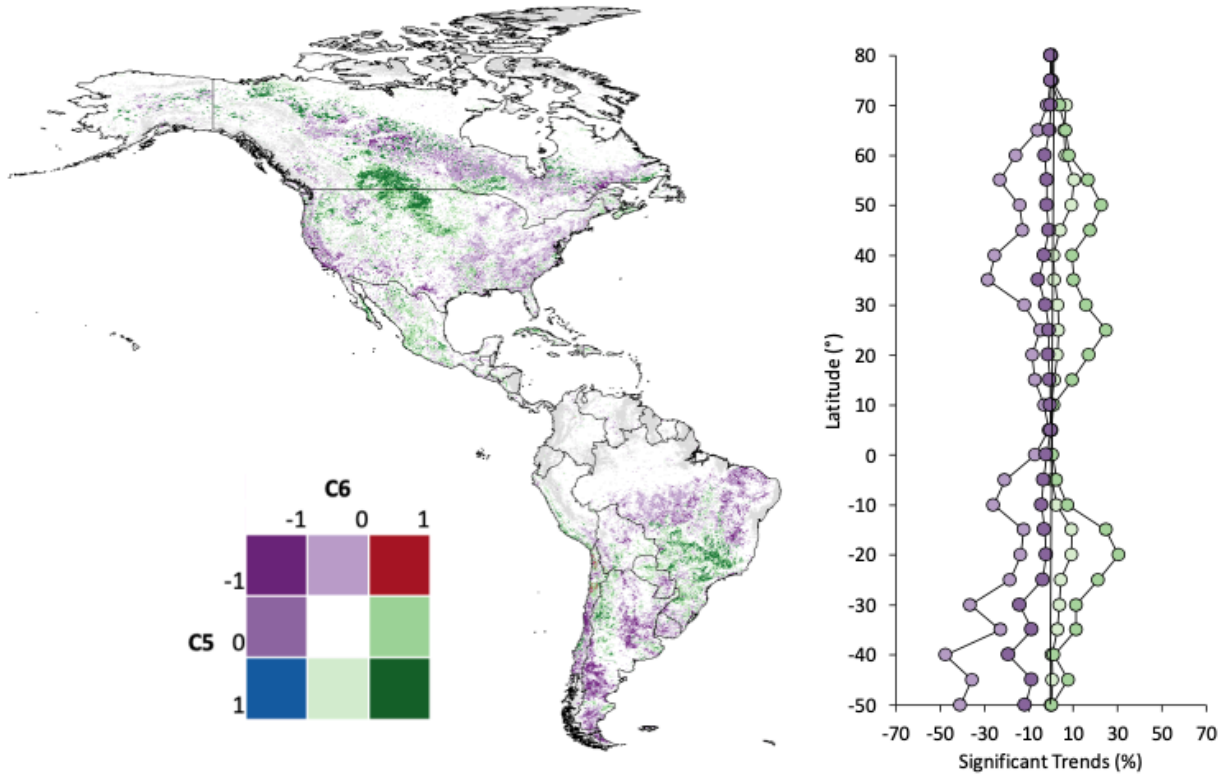

Figure 3: Comparison of MOD13C1 EVI C5 and C6. Nine different scenarios are presented. The greatest areas of discordance are stable in C5 and positive in C6 (medium green), but there are also several areas that are stable in C5 and negative in C6 (medium purple). Grey areas have insufficient data to support trend detection. NDVI results are very similar (not shown). The latitude graph reveals the total percentage of positive and negative trends in C5 (light purple and

light green) and C6 (dark purple and dark green). Note that the trends in the latitude graph are not stacked.

3.3 MOD11C2

In addition to trend analysis on the vegetation indices, we have also completed the same analysis for the MODIS Terra LST (Figures 4 and 5). The LST data do not reveal the pattern of discordances similar to the VI data, but instead show high concordance across both daytime and nighttime LST for the two collections. The trend analysis reveals 84.6% concordance for daytime LST and 77.8% for nighttime LST between C5 and C6, with 12% and 17% missing data, respectively (Table 6). Only 3.2% of daytime and 5% of nighttime LST trends exhibit discordance between collections. For these changed daytime trends, 7% goes from negative in C5 to no trend in C6, 16% goes from no trend to negative, 34% from no trend to positive, 42% from positive to no trend, and less than 1% goes from either positive to negative or the reverse. Thus, half the significant daytime LST trends in C5 exhibit no trend in C6. For nighttime trends, the number is even larger: 65% of significant nighttime LST trends in C5 show no trend in C6, with the most common shift being from positive in C5 to no trend in C6. However, for both daytime and nighttime LST, more than one-third of the shift comes from no trend in C5 to positive trend in C6 (Table 6).

The high concordance between the two daytime LST collections is also visible in Figure 5. There are two daytime warming peaks, one around 45°S and one around 10°S. More discrepancies appear between the nighttime LST collections. There are three nighttime warming peaks: 35°S, 5°S and 30°N. While the daytime warming is almost identical between the two collections, we find some difference in the nighttime warming peak around 5°S, where C5 revealed warming in a larger percentage of the pixels (20%) than C6 (12%). There are two very small

daytime cooling peaks, around 20°S and around 20°N, again both collections agree on the location of these peaks. Very few pixels with nighttime cooling trends appear in either collection.

Table 6: MOD11C2 trend comparison results (% of all pixels) between trends C5 and C6 for both daytime and nighttime LST.

MOD11C2 Day	**C6**			**Missing data = 12.20**
C5	*Negative*	*No Trend*	*Positive*	*Total*
Negative	0.55	0.23	0.00	0.78
No Trend	0.52	81.51	1.09	83.12
Positive	<0.01	1.39	2.51	3.90
Total	1.07	83.13	3.60	Concordance = 84.57
MOD11C2 Night	**C6**			**Missing data = 17.11**
C5	*Negative*	*No Trend*	*Positive*	*Total*
Negative	0.01	0.01	<0.01	0.02
No Trend	0.03	75.07	1.75	76.85
Positive	<0.01	3.26	2.76	6.02
Total	0.04	78.34	4.51	Concordance = 77.84

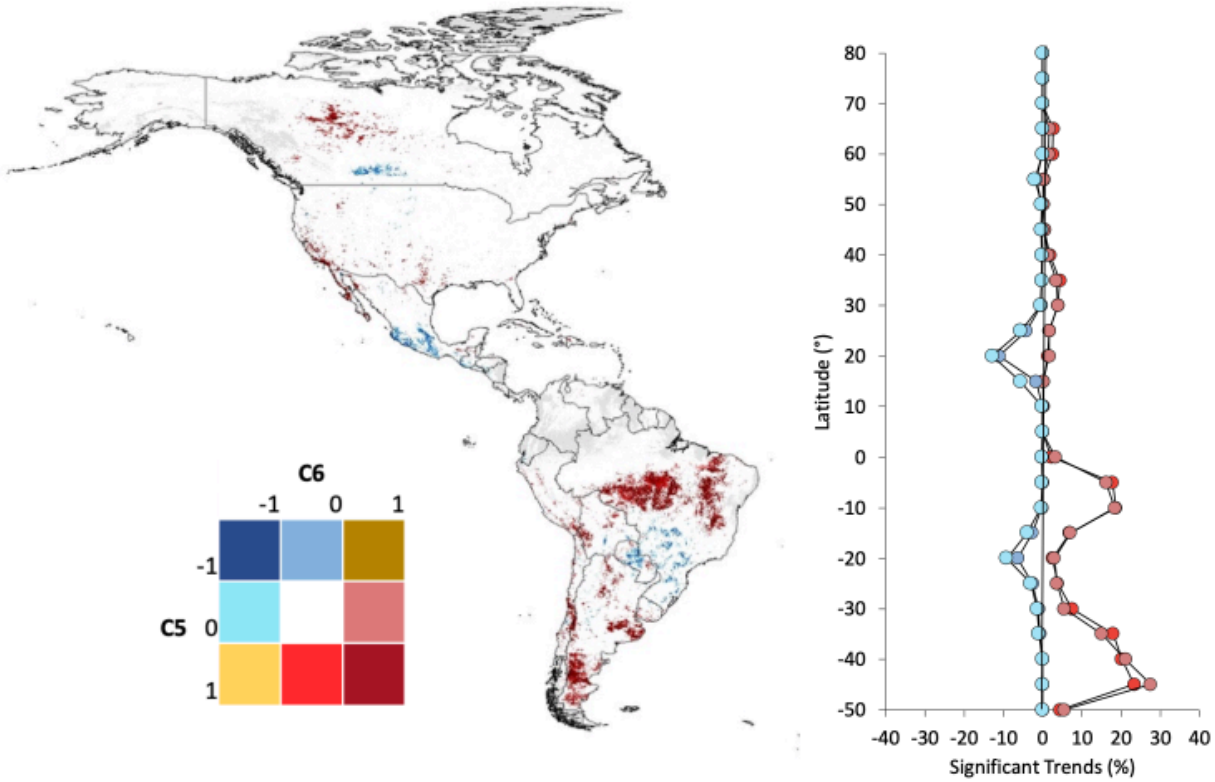

Figure 4: MOD11C2 daytime LST C5 and C6 comparison reveals less discordance in temperature than in vegetation indices. The most prevalent discordant scenario is a positive trend in C5 and a no detected trend in C6 (bright red). Note that the trends in the latitude graph are not stacked.

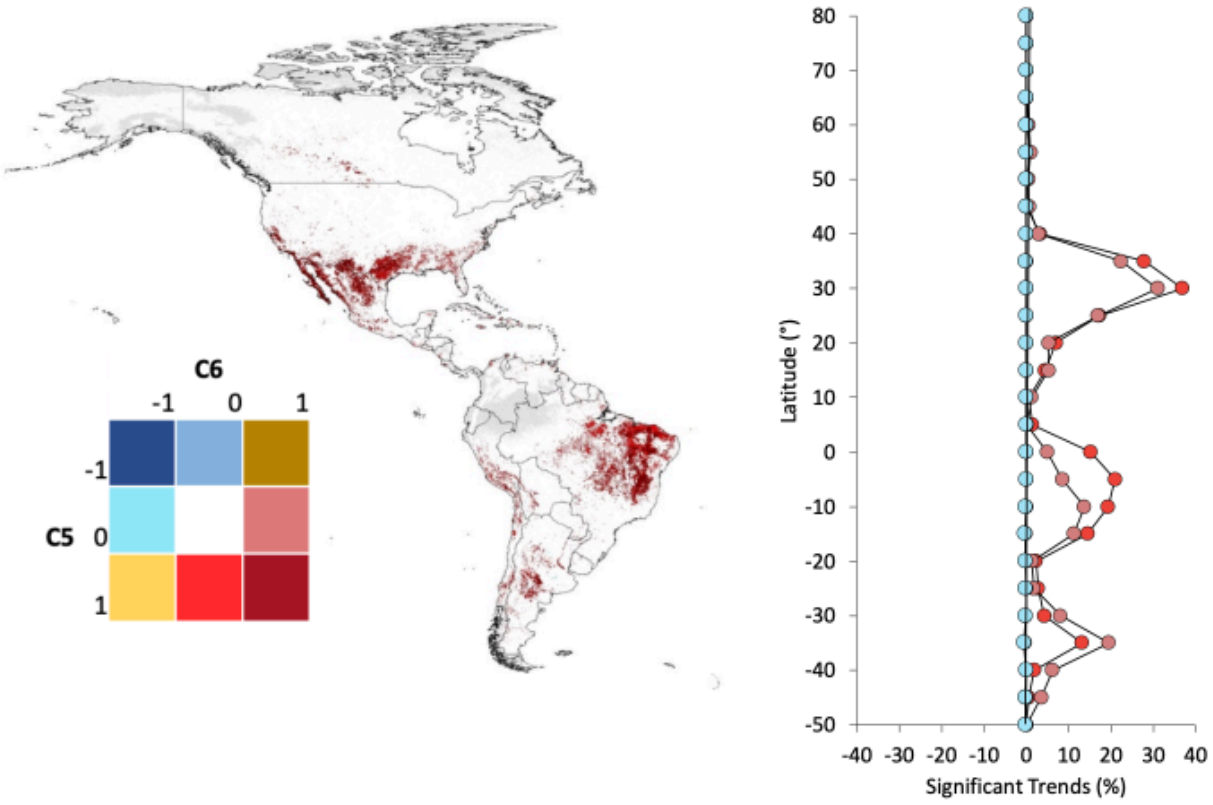

Figure 5: MOD11C2 nighttime LST C5 and C6 comparison reveals less discordance in temperature than in vegetation indices. The most prevalent discordant scenario is a positive trend in C5 and a no detected trend in C6 (bright red). Note that the trends in the latitude graph are not stacked.

3.4 Changes by Land Cover class

When we evaluate the trend results by land cover class, we can see the percentage of significant positive trends are higher in C6 for all classes for both MCD43C4 and MOD13C1 (Figure 6). In addition, the percentage of significant negative trends, based on data from C6, are lower for all land cover classes in both datasets. For the MCD43C4 data, we find that the percentage of negative trends is consistently lower than the percentage of positive trends across all classes, except for the Urban/Built-up areas that reveal approximately the same percentage of positive and negative trends. The MOD13C1 EVI trend results by land cover exhibit more variability between classes, with much higher percentages of positive trends in croplands,

compared to, for example, evergreen broadleaf forests. The MOD13C1 data also display major differences in the percentage of negative trends for the woody savannas between collections.

When evaluating the MOD11C2 LST trends by land cover class, we find the most cooling trends in croplands (7.2% in C5 vs. 8.0% in C6) followed by grasslands (1.8% vs. 2.3%), savannas (1.4% vs. 2.0%), and urban areas (1.2% vs. 1.9%). The percentage of daytime cooling in the other three classes was less than 0.5% (Figure 7). The daytime warming trends were highest in urban areas (5.5% vs. 5.7%) followed by evergreen broadleaf forests (5.1% vs. 3.8%), savannas (4.9% vs. 4.7%), and croplands (4.8% vs. 3.4%). Only for urban areas and open shrublands did we find more daytime warming in C6 than in C5. We find no nighttime cooling in either collection, but there is a considerable amount of nighttime warming for all classes. For example, the urban, cropland, open shrubland, and grassland classes reveal nighttime warming for more than 10% of each class; however, the nighttime warming is more prevalent in C5 than in C6, except for the open shrubland class (Figure 7).

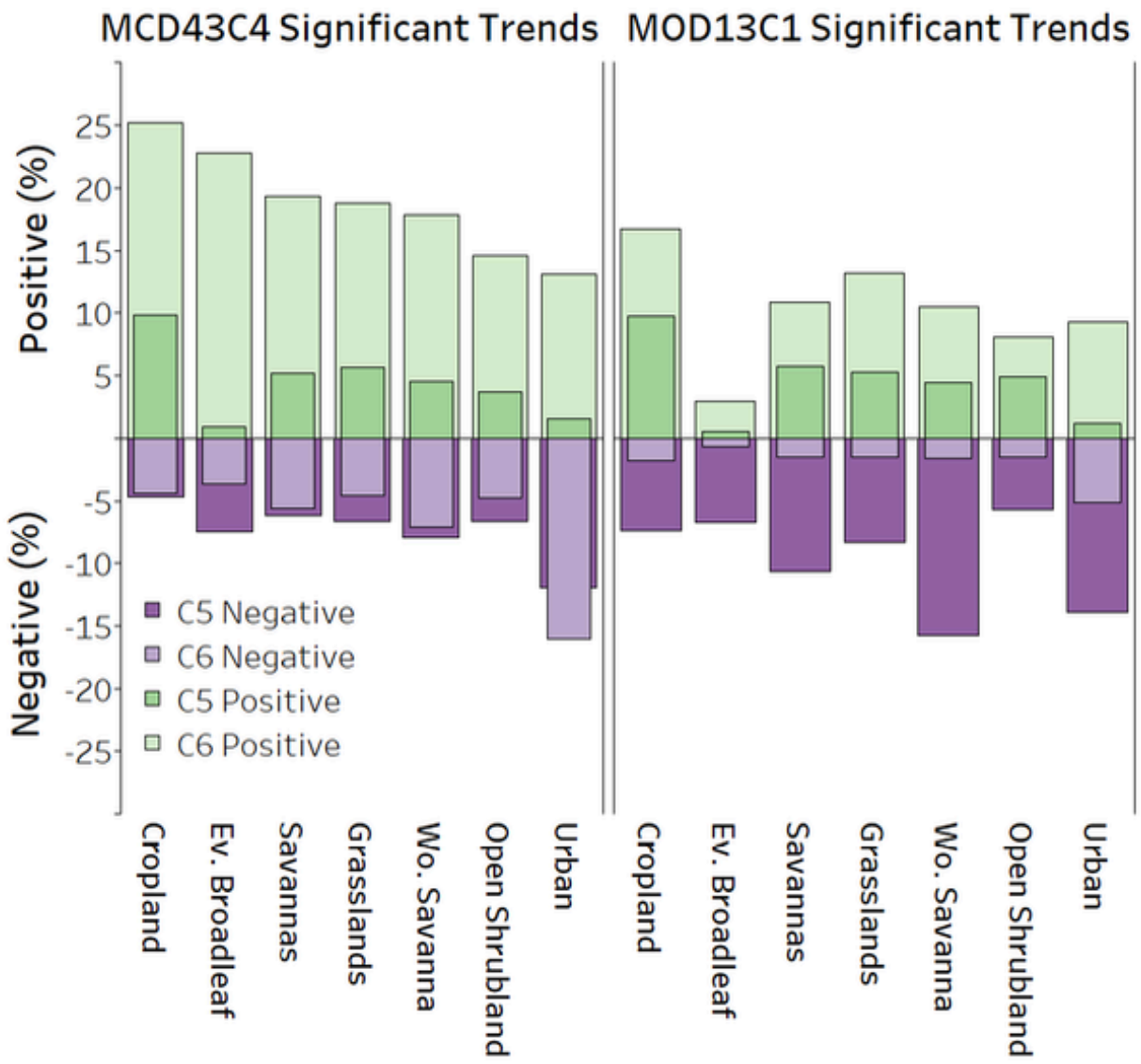

Figure 6: Percentage of significant trends by land cover class for EVI from MCD43C4 and MOD13C1. Land cover classes are ordered by percentage of positive trends in C006 for the MCD43C4 data. Croplands exhibit the largest percentage of significant positive trends in C006 and Urban the smallest. Urban reveals the largest significant negative trends for both C005 and C006 in MCD43C4. However, for MOD13, wooded savanna, the most arid cover class considered, exhibits a larger percentage of significant negative trends in C005.

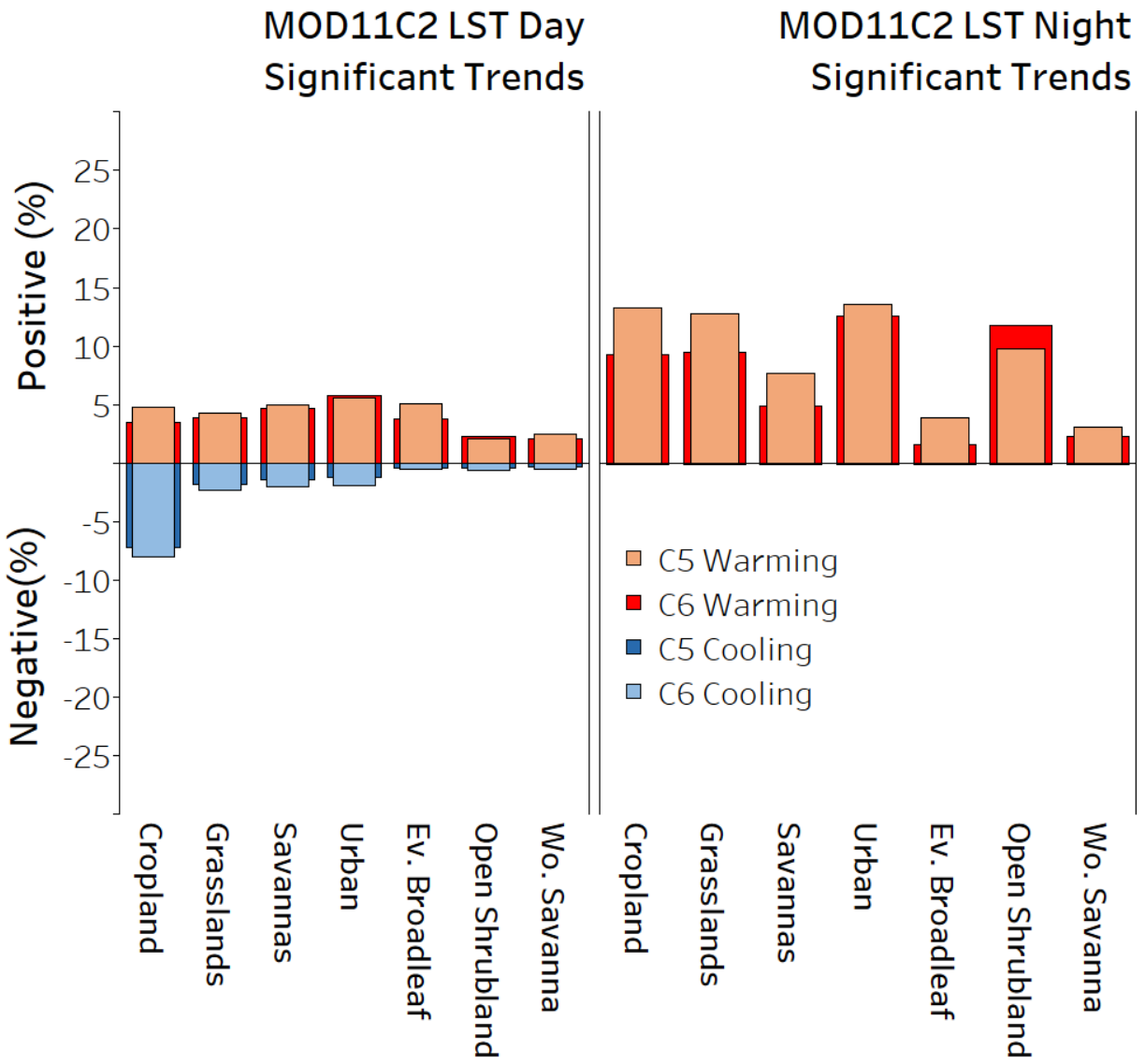

Figure 7: Percentage of significant trends by land cover class for the daytime and nighttime LST data from the MOD11C2 product.

3.5 Joint Trend Analysis: EVI and LST

Table 7 provides an overview of the joint trend analysis for the EVI from the MCD43C4 product and the daytime temperature from the MOD11C2 product for C5 and C6. Note that in this joint analysis, trend alignment appears as areas with either browning and warming or greening and

cooling. Missing data is 25.55% in C5 and 25.56% in C6. Trend alignment between the datasets in 62.53% in C5 and 55.88% in C6. In other words, we find trend misalignment between the datasets in 11.92% of the C5 data and 18.53% of the C6 of the data. Most misalignments appear in areas with a changing vegetation index trend that reveal no trend in the LST data. For C5, we find that 10% of the pixels fall into this category, with 7.06% of the pixels revealing a negative vegetation trend and no trend in LST; whereas, 2.94% of the pixels revealing a positive vegetation trend but no trend in LST. For C6, the total percentage of pixels in this category increased to 15.88% with 2.62% of the pixels exhibiting browning without LST change, and 13.26% of the pixels exhibiting greening without a temperature change. We find that 24.96% of the pixels with significant browning in C5 also show significant warming, compared to 30.53% in C6. On the other hand, we find that 10% of the pixels in C5 exhibit with significant greening also exhibit significant cooling, but just 5.6% for C6. In C5, only 0.78% of the Western Hemisphere is significantly cooling with 45% of this cooling area corresponding to areas with significant greening. On the other hand, analysis of C5 reveals that 3.84% of North and South America is significantly warming, with 61.3% of those pixels also exhibiting significant browning. Interestingly, for C6, we find that 1.06% of the study area is cooling, with 75% of those pixels also showing significant greening. Thus, we find more cooling in C6, and the cooling corresponds with more greening than in C5. However, C6 reveals that 3.54% of the study region has significant warming, but only 32.7% of the warming areas also exhibit browning. While we find slightly less area with significant warming, these warming patches in C6 appear to be less strongly linked to browning than in C5. Figure 8 displays the joint vegetation and temperature trends for C5 (Figure 8 top) and C6 (Figure 8 bottom). The darker toned areas are the regions where the vegetation index and the LST both exhibit significant, aligned trends in the expected directions. It is interesting to note the increase in greening and decrease in browning between C5 and C6 are easily recognizable

in the figure, but that the regions where both the vegetation index and the LST show significant, concordant, trends appear relatively stable in C5 and C6. This pattern is most likely the result of the lack of major changes between C5 and C6 for the LST data. We find comparable responses for the nighttime temperatures (Table 7).

Table 7: Combined EVI and LST daytime trends. Note that the shaded trends reveal areas of trend alignment, since increases in vegetation typically are related with cooling, and decreases in vegetation are often linked to warming. Final total percentages do not fully match total percentages from previous tables as a result of the slightly different combined missing data mask for EVI and LST.

C5	**MOD11C2 Daytime**			**Missing data = 25.55**
MCD43C4 EVI	*Cooling*	*No Trend*	*Warming*	*Total*
Negative	0.02	7.06	2.35	9.43
No Trend	0.41	59.83	1.45	61.69
Positive	0.35	2.94	0.03	3.33
Total	0.78	69.83	3.84	Alignment= 62.53
C6	**MOD11C2 Daytime**			**Missing data = 25.56**
MCD43C4 EVI	*Cooling*	*No Trend*	*Warming*	*Total*
Negative	0.01	2.62	1.16	3.79
No Trend	0.25	53.93	2.25	56.44
Positive	0.79	13.26	0.13	14.18
Total	1.06	69.81	3.54	Alignment = 55.88

Table 8: Combined EVI and LST nighttime trends. Note that the shaded trends reveal areas of trend alignment, since increases in vegetation typically are related with cooling, and decreases in vegetation are often linked to warming. Note: there is virtually no nighttime cooling in either collection.

C5	**MOD11C2 Nighttime**			**Missing data = 27.85**
MCD43C4 EVI	*Cooling*	*No Trend*	*Warming*	*Total*
Negative	0.00	8.06	1.35	9.41
No Trend	0.01	55.30	4.45	59.46
Positive	0.00	3.16	0.17	33.33
Total	0.02	66.52	5.67	Alignment = 56.65
C6	**MOD11C2 Nighttime**			**Missing data = 27.85**
MCD43C4 EVI	*Cooling*	*No Trend*	*Warming*	*Total*
Negative	0.00	3.32	0.45	3.77
No Trend	0.02	51.37	3.09	54.48
Positive	0.01	13.21	0.68	13.91
Total	0.04	67.90	4.22	Alignment = 51.83

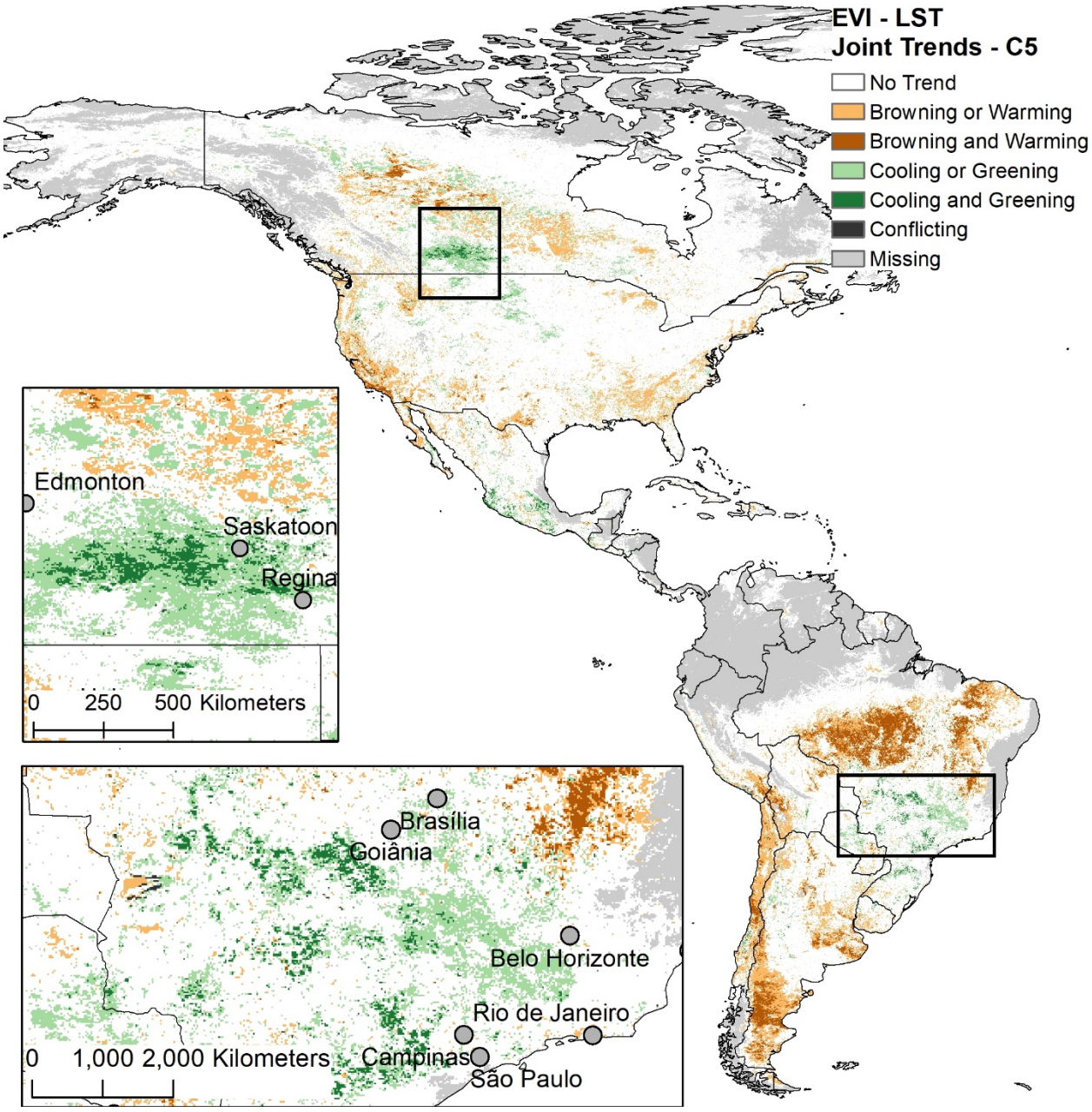
EVI - LST
Joint Trends - C5
No Trend
Browning or Warming
Browning and Warming
Cooling or Greening
Cooling and Greening
Conflicting
Missing
Edmonton
Saskatoon
Regina
0 250 500 Kilometers
Brasília
Goiânia
Belo Horizonte
Rio de Janeiro
Campinas
São Paulo
0 1,000 2,000 Kilometers

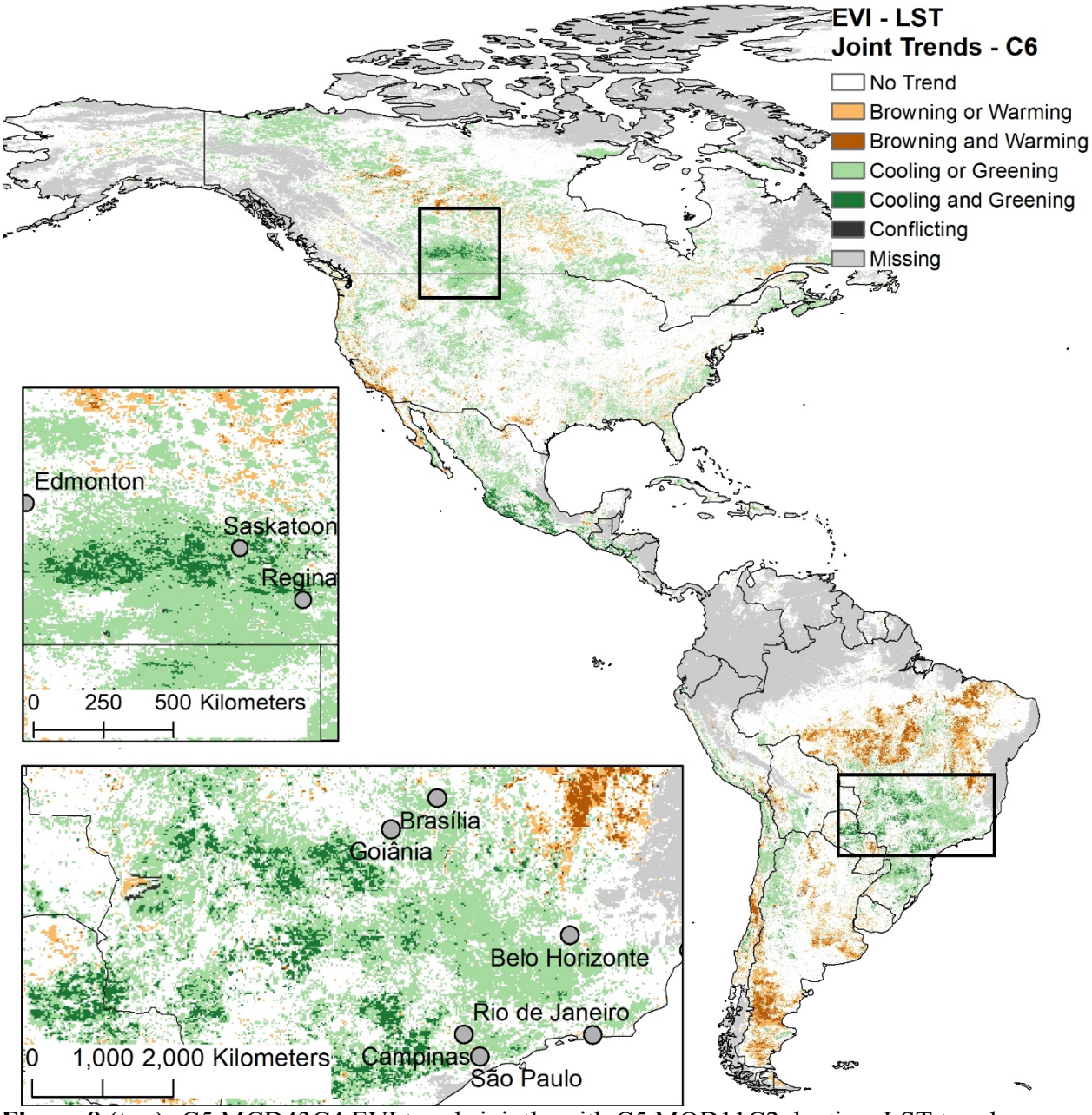

Figure 8 (top): C5 MCD43C4 EVI trends jointly with C5 MOD11C2 daytime LST trends. **(bottom)** C6 MCD43C4 EVI trends jointly with C6 MOD11C2 daytime LST trends. Conflicting trends indicate areas where increasing temperatures are found with increasing vegetation and vice versa.

3.6 Trend results by human influence

We analyzed the trend results by human influence class (1- 64) to investigate if areas with greater human influence revealed different trend results. We present these results in Figures 9, 10,

and 11, showing the percentages of trends found in C5 and C6, with the strength of the human influence index (1-64) divided into four different categories represented by different sized points. Figure 9 demonstrates that there is a greater percentage of negative trends in C5 and more positive trends in C6. It is also interesting to note that regions of low human influence (HII<7) have a greater relative percentage of negative trends indicated by the larger points. On the flip side, the percentages of positive trends in C6 are approximately 3-7 times higher than the percentages of positive trends in C5. The distribution of the different sized points for the positive trends indicate no clear pattern with respect to the different human influence categories.

Figure 10 demonstrates that percentages of positive and negative trends in the daytime and nighttime LST data for C5 and C6 are very similar. The daytime LST data reveal both positive and negative trends, with both sets plotted close to the identity line. The nighttime LST data exhibit only significant positive (warming) trends in both C5 and C6, with most of the human influence categories plotting just below the identity line, indicating that the percentage of significant trends found is slightly higher in C5 than in C6. Interestingly, the negative trends appear greater for the areas with the lowest human influence (HII<7) and the difference between C5 and C6 is greatest for those areas. These areas can be found in central Brazil and northern Canada.

Figure 11 shows the results for the selected four sinusoidal tiles—h09v05, h12v04, h13v02, and h13v10—of the MCD43A4 product, which cover portions of the southwestern US (table S2), eastern US/Canada Great Lakes region (table S3), northern Canada (table S4), and the Brazilian cerrado or savanna (table S5), respectively. We use these data to evaluate how results may differ between the spatial resolution of 0.05° and 500 m. We found the 500 m trend results from three of the four regions were relatively consistent with the trends from the coarser resolution data. However, the tile h13v02 covering the Canadian tundra exhibited different

results, perhaps because the extent of human influence is less than what we see, on average, across the western hemisphere and the other tiles.

Similar to the 0.05° dataset, we found that a majority of points lie above the identity line indicating that C6 presented more positive trends, while C5 had more negative trends. Among the negative trends in the Great Lakes region (tile h12v04), the greatest disparity between the collections occurred in areas with the highest human influence (figure 11). Out of our four tiles analyzed, this region also had 3.5 times as many C6 positive trends as in C5, which was the greatest disparity between collections among the four regions (table S3). The Brazilian cerrado (tile h13v10) showed that areas with high human influence had the more differences in negative trends between collections (table S5). Interestingly, a majority of positive trends in areas with the highest human influence (HII>30) in the Great Lakes and in the cerrado regions exhibited the lowest disparities between collections.

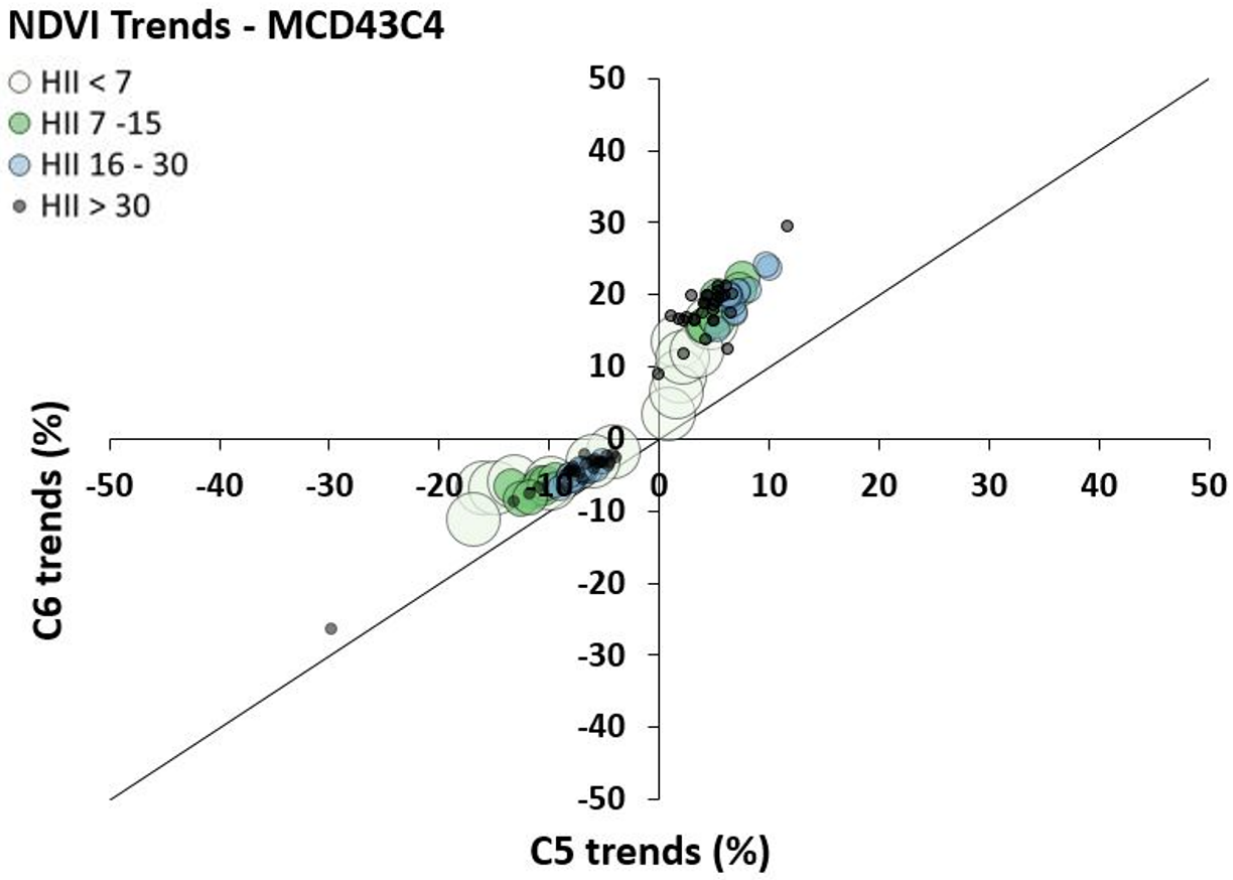

Figure 9: Differences between C5 and C6 based on MCD43C4 NDVI positive and negative trend percentages for each degree of human influence (1-64; indicated by dot size and color). All the points are above the identity line, demonstrating a greater percentage of negative trends in C5 and more positive trends in C6. Colors correspond with Figure 1.

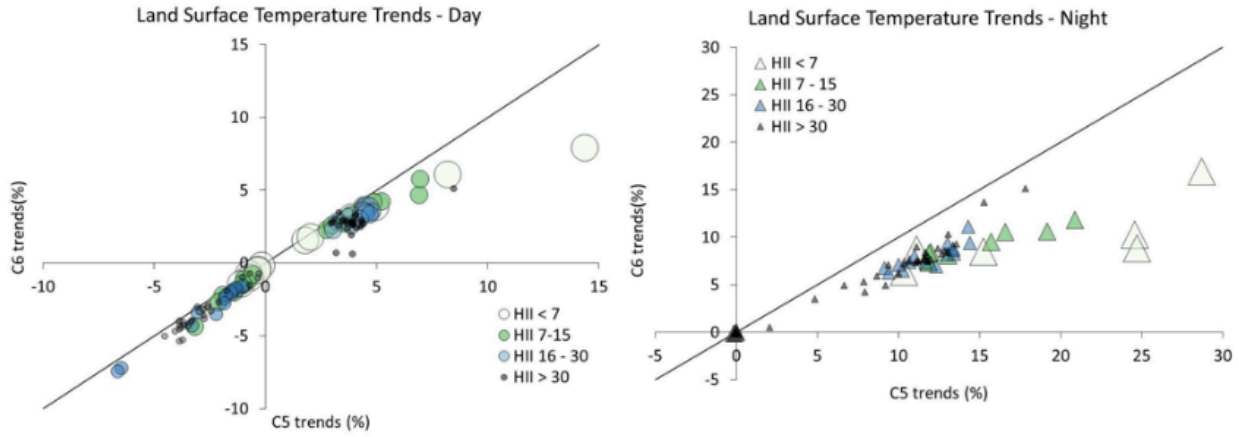

Figure 10: Differences between C5 and C6 based on MOD11C2 daytime (left) and nighttime (right) LST positive and negative trends for each degree of human influence (1-64; indicated by dot size and color). Daytime trends are split between both cooling (negative) and warming (positive). Nighttime trends reveal only warming. Human influence affects these trends, with the most extensive areas of daytime warming generally have less human influence (larger dots/triangles). There is less nighttime warming for areas with high human influence (smaller triangles) in both collections. Colors correspond with Figure 1.

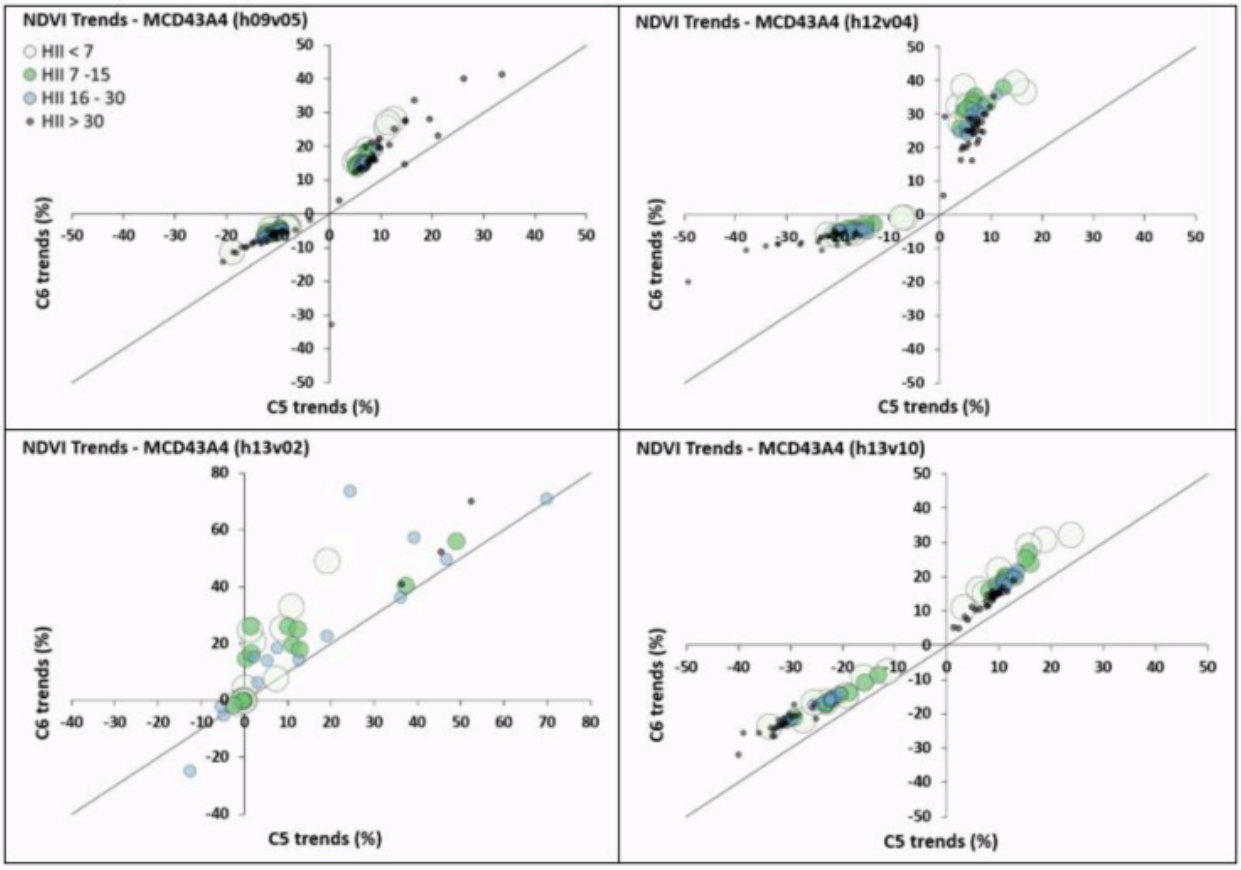

Figure 11: Differences between C5 and C6 based on MCD43A4 NDVI positive and negative trend percentages for each degree of human influence (1-64; indicated by dot size and color). Three of the sinusoidal tiles (h09v05, h12v04, and h13v10) are consistent with Figure 9, having all points above the identity line. This indicates that there is a greater percentage of negative trends in C5 and more positive trends in C6. However, there is unique clustering for each region. For example, in tile h13v10, the points representing HII>30, on average, have the highest percentages of negative trends.

4. Discussion

4.1 Trends in MODIS Vegetation Indices in Collections 5 and 6

As early as 2012, Wang et al. (2012) reported on the impact of sensor degradation on MODIS collection 5 NDVI time series from Terra. That paper demonstrated a nearly threefold difference in the percentage of negative trends derived from Terra compared to those derived from Aqua for the period 2002-2010 (17.4% vs. 6.7%). Here we have presented a thorough and careful analysis of the consistency between MODIS collections C5 and C6 for the western hemisphere for three different products: a combined product (MCD43C4), which uses data collected from Terra and

Aqua, and two products generated solely from Terra (MOD11C2 and MOD13C1). In addition, we extended the VI trend comparison to four diverse MODIS tiles at 500 m resolution (MCD43A4). There are known differences between the sensors on these two satellites due to the pre-launch event, the opening of the solar door and the closing of the solar door screen after launch, which caused degradation as summarized in Table S1 (Wang *et al.*, 2018). It is important to keep in mind that the percentage of missing data was slightly different for all three products. The trend percentages we found for the vegetation indices appear comparable to the percentage of negative trends reported earlier (Wang *et al.*, 2012). Detsch *et al*. (2016) found that with the improvements made for C6, data retrieved from the Terra satellite displayed more greening compared to data from Aqua. Along with a possible overcompensation that was meant to correct Terra degradation, the time of day the sensor collects data should also be considered as to why Terra records more greening trends: MODIS Terra benefits from a mid-morning time observation that results in fewer clouds compared to Aqua's early afternoon overpass (Lyapustin *et al.*, 2014).

Zhang *et al.* (2017) suggested that previous studies of temporal vegetation trends based solely on Terra C5 data might need to be re-investigated. Over the past decade, several studies discussed the browning of Earth, presenting a variety of reasons for these browning trends. One study found large portions of land that revealed browning in Terra C5, for example in tropical regions, without showing these trends in Terra C6 (Zhang *et al.*, 2017), although that paper investigated only the annual vegetation index maxima, when differences should be least apparent. One paper specifically compared the results of MOD13 C5 NDVI trends with trends observed in the AVHRR GIMMS NDVI data for the 11-year period from 2000-2010 (Fensholt & Proud, 2012). For the Western Hemisphere (North and South America), they found positive NDVI trends for 4.73% of the study area in the MOD13 data compared to 6.52% for the GIMMS data. On the other hand, they found negative trends for 8.72% of the study region with MOD13 data and 4.33% with the

GIMMS data, indicating about twice the amount of negative trends in MOD13 compared to GIMMS and about 50% fewer positive trend pixels. It is apparent that most of the differences between these two datasets were found in South America where the MOD13 data revealed a negative NDVI trend for almost 25% of the land surface, while the GIMMS data revealed a negative NDVI trend for just 6.4% of the land surface. The differences were much smaller in North America, where the GIMMS data actually revealed a greater percentage of negative trends (3.4%) than the MOD13 data (1.4%).

Other papers also revealed that browning trends are not only found in the MODIS data, but also in the AVHRR dataset (de Jong *et al.*, 2011, de Jong *et al.*, 2012, Pan *et al.*, 2018). For example, between 2001 and 2013, Pan et al. (2018) found browning trends in 54.8%, 33.2% and 45.9% for the MODIS Terra C5, MODIS Terra C6 and GIMMS3g data respectively. Note that the global browning percentages found by Pan et al. (2018) are substantially higher (54.8% in C5 vs. 33.2% in C6) than the percentages reported here in table 3: 11.89% in C5 vs. 3.77% in C6. We believe this discrepancy likely arises from a variety of differences between the studies. First, we only investigate North and South America, as opposed to the entire globe. Second, we use consistent masking in our analysis, *e.g.*, we applied the same missing data mask to the C5 and C6 data for each product to ensure that we calculate our trend percentages based on the same number of pixels for both collections. Note, that while we apply the same missing data mask for the two collections, the missing data mask we apply to MOD13C1 is not the same for MCD43C4, because their product algorithms differ. Finally and perhaps most importantly, our trend detection method is much more conservative in estimating when a trend is significant ($p<0.01$) and is corrected for both seasonality and first-order serial autocorrelation, making the results yet more conservative. A comparison of time series trends from GIMMS3g, SeaWiFS, SPOT-VGT, and MODIS data revealed that for far northern latitudes these datasets agree in just 46% of the pixels, with 27.8%

of the land revealing greening in all datasets and 12.2% revealing browning in all datasets (Guay *et al.*, 2014). Both the GIMMS3g and the MODIS NBAR data showed browning in an additional 12.9% and 13.5% of the pixels, respectively, while the SPOT D10 data exhibited browning in only 2.7% additional pixels, with greening in an additional 18.5% of the pixels (Guay *et al.*, 2014). Global LAI trends have also been compared for MODIS C6, MERIS, and GEOV1 data, and the mean trends captured in these products agreed very well (Jiang *et al.*, 2017). The study also revealed a decreasing LAI trend for the MODIS C5 LAI data and demonstrated that the GLASS and GLOBMAP LAI products, both based on MODIS C5 reflectance, also revealed negative trends during the overlapping time period (2003-2011).

Large-scale climate oscillations are often considered as responsible drivers for global and regional vegetation trends (Bastos *et al.*, 2017, de Beurs *et al.*, 2018, Jiang *et al.*, 2017). Vegetation browning—perhaps spuriously detected—has been explained by droughts (de Jong *et al.*, 2012, Xu *et al.*, 2012), wildfires (Potter, 2018), insect damage (Sulla-Menashe *et al.*, 2018, Verbyla, 2011), and extreme climate events (Bjerke *et al.*, 2014). Drought, vapor pressure deficit, and growing season stress were reported as possible causes of browning in the boreal forests of Canada (de Jong *et al.*, 2012). Browning trends in high northern latitudes were confirmed by tree ring analysis (Beck & Goetz, 2011, Berner *et al.*, 2011, Lloyd & Bunn, 2007). NDVI from GIMMS AVHRR data also revealed strong negative trends in Argentina, which has been explained by the expansion of agriculture in this region (Viglizzo *et al.*, 2011).

Some suggest that although the calibration changes improve the correlation between data from the two sensors, the presence of more greening trends in Terra collection 6 could hint that there was an overcompensation in the calibration efforts, considering that Aqua has proven to be the more stable sensor (Detsch *et al.*, 2016, Zhang *et al.*, 2017). Fan and Liu (2016) suggest that land cover differences may play a more important role when comparing NDVI differences from

different moderate resolution sensors than, for example, atmospheric variations. Others have suggested that it is good practice to use an ensemble of different datasets when investigating land surface changes to allow for the identification of errors in data, as they found significant errors in the GIMMS3.0g dataset for Australia's drylands (Burrell et al. 2018; errors have been addressed in the GIMMS3.1g dataset).

4.2 Trends in MODIS LST in Collections 5 and 6

LST is a very important variable when modeling surface energy and water balance processes (Bindhu *et al.*, 2013). In addition, satellite derived LST measurements can be especially important in areas with a limited number of meteorological stations, such as the far northern latitudes. MODIS LST data are also often used to understand urban heat islands (*e.g.*, (Krehbiel & Henebry, 2016, Krehbiel *et al.*, 2017, Walker *et al.*, 2015, Fu and Weng, 2018), with some reporting on trends in urban LST (Benas *et al.*, 2017). There have not been many studies focusing on consistency of the MODIS LST products across collections. One paper concludes that MODIS LST C6 data provides more stable data than previous collections (Wongsai *et al.*, 2017). As summarized in Table S1, trend discordance between C5 and C6 LST predominantly occurs in LST retrieval over drylands. Interestingly, our land cover analysis reveals very little difference between collections for all land cover classes, except for the open shrubland class, the driest class considered. Open shrubland is also the only class where we now find a larger percentage of area with nighttime warming than in C5.

As with the MODIS VI data, there are authors who do not specifically address which MODIS collection was used in their analysis (Benas *et al.*, 2017, Williamson *et al.*, 2017).

5. Conclusions

There have been few papers discussing the discrepancy between C5 and C6 vegetation index data (Lyapustin *et al.*, 2014, Zhang *et al.*, 2017), and the major trend discordances between the two collections have received limited attention. As a result, even in 2018, there are still papers published based solely using C5 NDVI data (*e.g.*, Fang *et al.*, 2018), while others do not specify the collection of the data used (*e.g.,* Browning *et al.*, 2018, Murthy & Bagchi, 2018).

The aim of this study was to determine how the changes to the newly reprocessed MODIS collection (C6) would impact the VI and LST in comparison with the previous collection (C5). Our results revealed that while trend results from both the MOD13C1 and MCD43C4 data products, as well as results for NDVI and EVI exhibit broad concordance in significant trends, there were distinct differences between collections. We also demonstrated that the differences between C5 and C6 for the LST data are minor, allowing us to conclude that we do not expect major differences in the discussion around temperature trends as observed by MODIS sensors. Finally, we showed that the regions where both the vegetation index and the LST show significant, concordant trends are relatively stable in both C5 and C6, which demonstrates the advantage of jointly investigating land surface dynamics using more than one product.

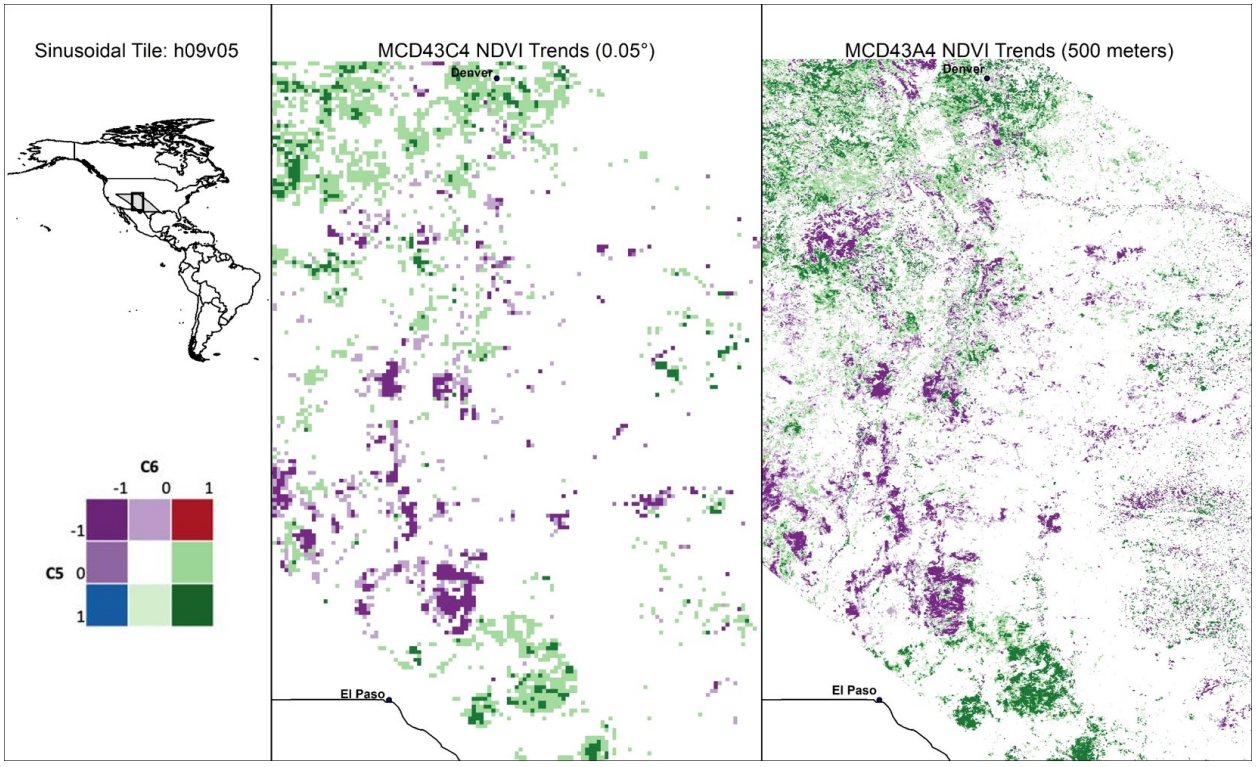

Figure 12: Comparison of trend detections in MCD43C4 and MCD43A4. From Table S2, it can be seen that there is good consistency between products but, as expected, the 500 m data show more trends and finer spatial detail.

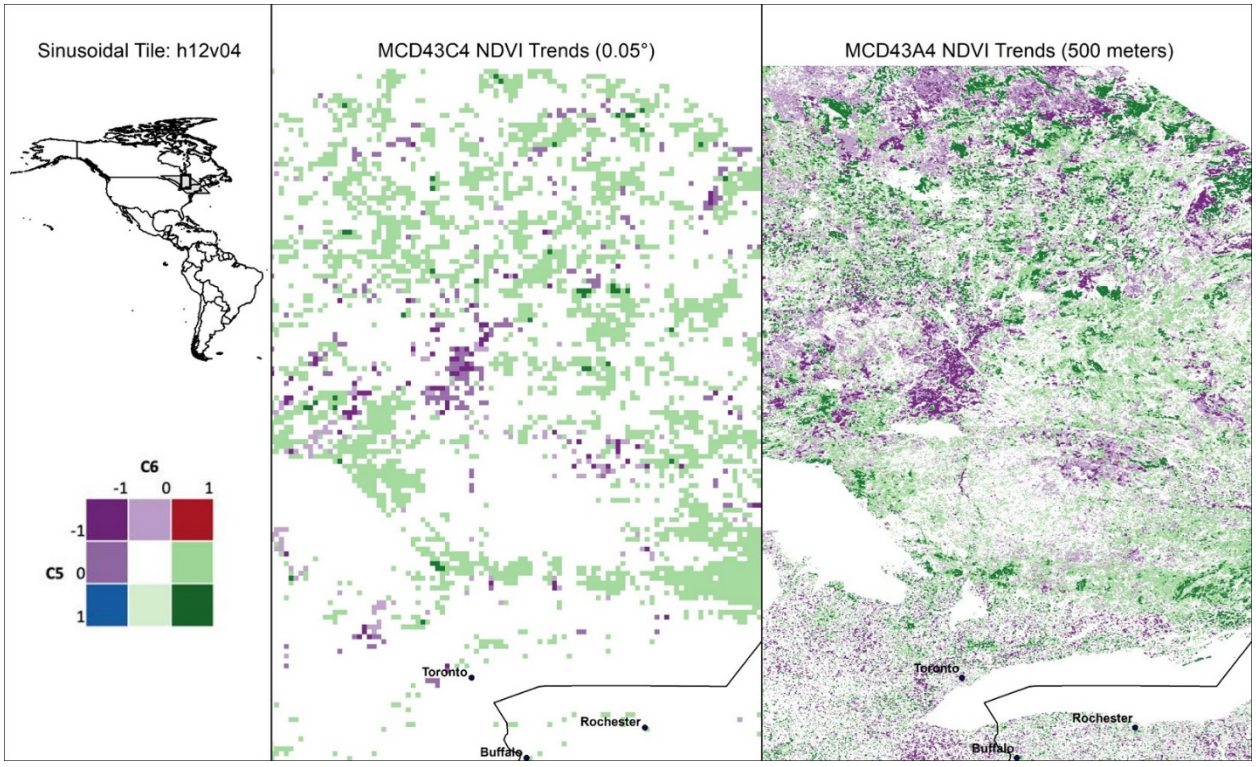

Figure 13: Comparison of trend detections in MCD43C4 and MCD43A4. From Table S3, it can be seen that there is good consistency between products but, as expected, the 500m data show more trends and finer spatial detail.

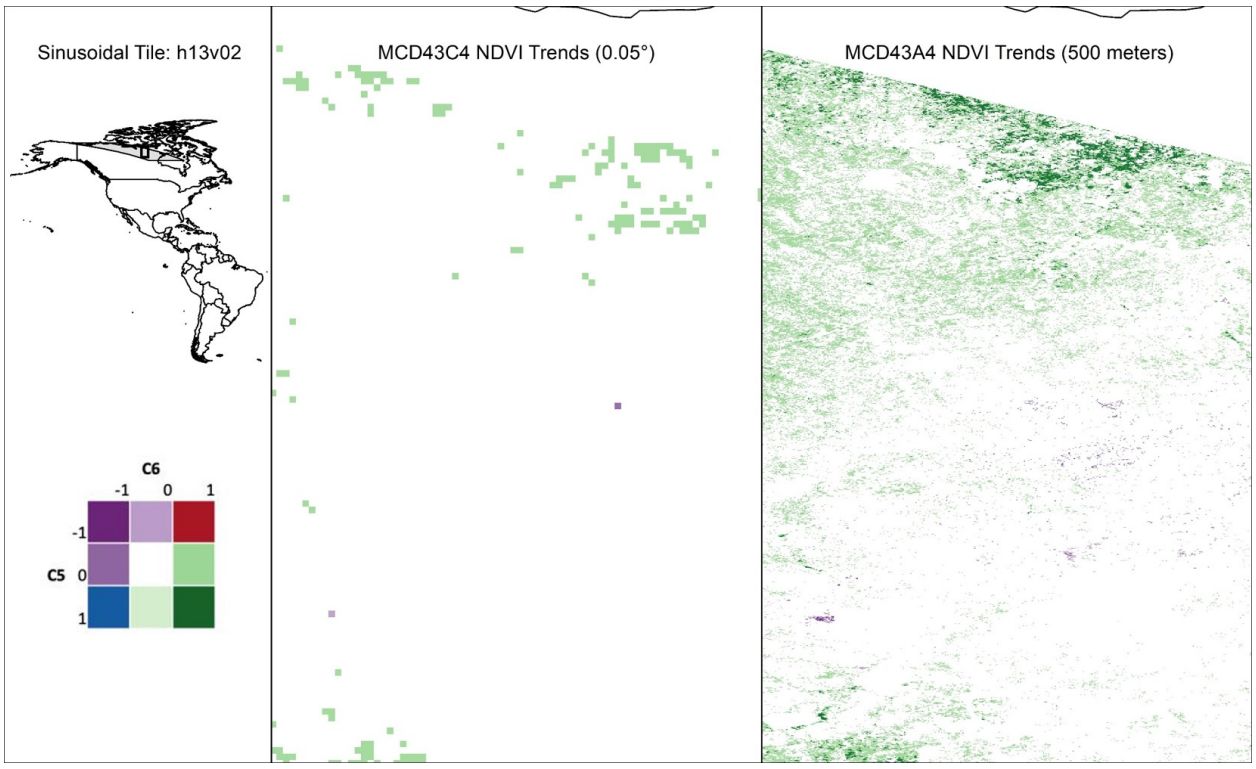

Figure 14: Comparison of trend detections by MCD43C4 and MCD43A4. From Table S4, it can be seen that there is good consistency between products but, as expected, the 500 m data show more trends and finer spatial detail.

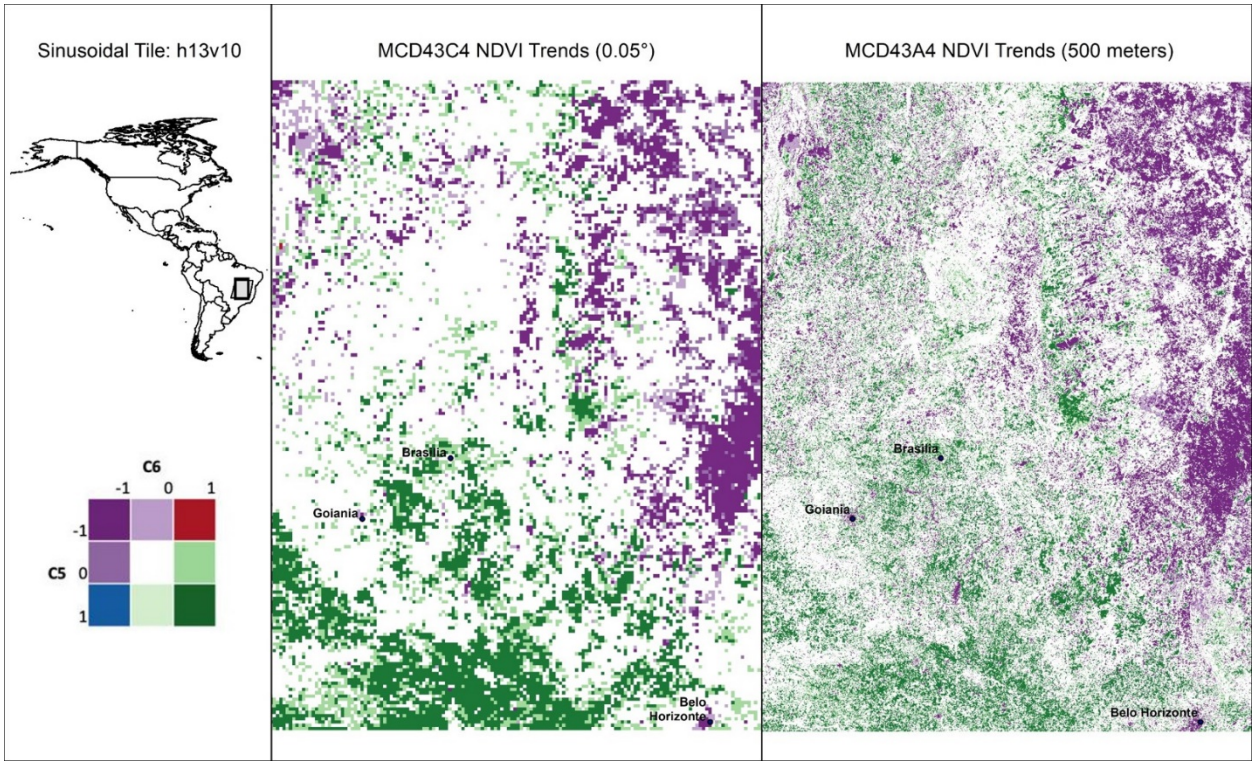

Figure 15: Comparison of trend detection in MCD43C4 and MCD43A4. From Table S5, it can be seen that there is good consistency between products but, as expected, the 500 m data show more trends and finer spatial detail.

Table S1: Product improvements from C5 to C6 for the selected products.

Product	Improvement
M{O|Y}D09	Three main improvements: solar diffuser degradation correction, response vs. scan angle look up table updates, polarization correction.
M{O|Y}D09 -lite	Improved aerosol retrieval and correction algorithms, refined snow, cloud, and cloud shadow detection algorithms.
MOD13C1	Gap filling for low quality data (Didan et al. 2015).
MOD13C1	Use of pre-composited surface reflectance data by combining two 8-day composites from MOD09A1 data. Since the compositing only retains high quality data, the VI algorithm is more likely to generate accurate results (Didan *et al.*, 2015).
MOD13C1	Modification of the constrained view angle maximum value composite (CV-MVC) to allow for a wider range of view angles. The product uses this larger set of observations and models the final result to nadir view, and the new maximum value composite approach compares the observations with the highest NDVI and selects the observation which is closest to nadir. This approach is taken to minimize the BRDF effects (Didan *et al.*, 2015).
MOD13C1	An updated and more robust 2-band EVI backup algorithm that enables the EVI to be calculated using the red and NIR bands only if it is not ideal to use the blue band. The blue band is sensitive to clouds/snow and ice cover, and these conditions cause the EVI to be extremely high and will produce erroneous values. The 2-band backup algorithm does not consider the blue band but maintains the advantages of using the EVI (Didan *et al.*, 2015).
MCD43C4	Switched input data to L2G-Lite surface reflectance data (Schaaf, 2018).
MCD43C4	The final product is now generated daily based on 16 days of data. For this paper, we selected every eighth composite to match the 8-day temporal resolution of C5.
MCD43C4	Improved quality and increased retrievals at high latitudes from use of all available observations, resulting in fewer missing data. Improved backup database for poorer quality retrievals (Wang *et al.*, 2018).
MCD43C4	Expanded the quality and uncertainty values.
MOD11C2	Cloud contaminated pixels are removed (Wan, 2014).
MOD11C2	The split-window algorithm that is used to derive land surface temperature values is improved for bare soil regions (Duan *et al.*, 2017, Duan *et al*., 2018, Duan *et al*., 2019).
MOD11C2	Day/night algorithm is improved to enhance the LST accuracy over deserts.

Table S2: MCD43A4 (top) and MCD43C4 (bottom) trend comparison results (% of all pixels) between C5 and C6 for NDVI. These results represent the percentage of trends within the sinusoidal tile for each product.

Tile: h09v05 MCD43A4 NDVI	**C6**			
C5	*Negative*	*No Trend*	*Positive*	*Total*
Negative	4.95	5.67	0.01	10.63
No Trend	0.06	73.06	9.94	83.06
Positive	0.00	0.14	6.16	6.30
Total	5.01	78.87	16.11	Concordance = 84.17
MCD43C4 NDVI	**C6**			
C5	*Negative*	*No Trend*	*Positive*	*Total*
Negative	2.36	2.88	0.00	5.24
No Trend	0.20	80.88	10.63	91.71
Positive	0.00	0.02	3.02	3.04
Total	2.56	83.78	13.65	Concordance = 86.26

Table S3: MCD43A4 (top) and MCD43C4 (bottom) trend comparison results (% of all pixels) between C5 and C6 for NDVI. These results represent the percentage of trends within the sinusoidal tile for each product.

Tile: h12v04 MCD43A4 NDVI	**C6**			
C5	*Negative*	*No Trend*	*Positive*	*Total*
Negative	3.88	10.35	0.11	14.34
No Trend	0.14	61.78	16.94	78.86
Positive	0.00	0.02	6.79	6.81
Total	4.02	72.15	23.84	Concordance = 72.45
MCD43C4 NDVI	**C6**			
C5	*Negative*	*No Trend*	*Positive*	*Total*
Negative	0.63	3.43	0.02	4.08
No Trend	0.75	78.49	15.36	94.6
Positive	0.00	0.03	1.30	1.33
Total	1.38	81.95	16.68	Concordance = 80.42

Table S4: MCD43A4 (top) and MCD43C4 (bottom) trend comparison results (% of all pixels) between C5 and C6 for NDVI. These results represent the percentage of trends within the sinusoidal tile for each product.

Tile: h13v02 MCD43A4 NDVI	**C6**			
C5	*Negative*	*No Trend*	*Positive*	*Total*
Negative	0.04	0.10	0.00	0.14
No Trend	0.03	71.58	18.87	90.48
Positive	0.00	0.35	9.04	9.39
Total	0.07	72.03	27.91	Concordance = 80.66
MCD43C4 NDVI	**C6**			
C5	*Negative*	*No Trend*	*Positive*	*Total*
Negative	0.00	0.01	0.00	0.01
No Trend	0.02	81.62	18.17	99.81
Positive	0.00	0.00	0.18	0.18
Total	0.02	81.63	18.35	Concordance = 81.80

Table S5: MCD43A4 (top) and MCD43C4 (bottom) trend comparison results (% of all pixels) between C5 and C6 for NDVI. These results represent the percentage of trends within the sinusoidal tile for each product.

Tile: h13v10 MCD43A4 NDVI	**C6**			
C5	*Negative*	*No Trend*	*Positive*	*Total*
Negative	16.07	7.26	0.01	23.34
No Trend	0.60	55.77	8.24	64.61
Positive	0.00	0.31	11.74	12.05
Total	16.67	63.34	19.99	Concordance = 83.58
MCD43C4 NDVI	**C6**			
C5	*Negative*	*No Trend*	*Positive*	*Total*
Negative	10.21	3.69	0.01	13.91
No Trend	3.38	63.28	8.06	74.72
Positive	0.00	0.03	11.33	11.36
Total	14.09	67.00	19.4	Concordance = 84.82

Acknowledgements

This research was supported, in part, by the NASA Science of Terra & Aqua project NNX14AJ32G entitled *Change in our MIDST: Detection and analysis of land surface dynamics in North and South America using multiple sensor datastreams*, and the Center for Global Change and Earth Observations at Michigan State University. All MODIS data products used in this study were retrieved from the online Data Pool, courtesy of the NASA Land Processes Distributed Active Archive Center (LP DAAC), USGS/Earth Resources Observation and Science (EROS) Center, Sioux Falls, South Dakota, https://lpdaac.usgs.gov/data_access/data_pool. We thank the anonymous reviewers for helping us to improve the clarity and coherence of our research presentation.

References

Bastos A, Ciais P, Park T *et al.* (2017) Was the extreme Northern Hemisphere greening in 2015 predictable? Environmental Research Letters, **12**, 044016.

Beck PS, Goetz SJ (2011) Satellite observations of high northern latitude vegetation productivity changes between 1982 and 2008: ecological variability and regional differences. Environmental Research Letters, **6**, 045501.

Belward AS, Skoien JO (2015) Who launched what, when and why; trends in global land-cover observation capacity from civilian earth observation satellites. ISPRS Journal of Photogrammetry and Remote Sensing, 103, 115-128.

Benas N, Chrysoulakis N, Cartalis C (2017) Trends of urban surface temperature and heat island characteristics in the Mediterranean. Theoretical and Applied Climatology, **130**, 807-816.

Berner LT, Beck PS, Bunn AG, Lloyd AH, Goetz SJ (2011) High-latitude tree growth and satellite vegetation indices: Correlations and trends in Russia and Canada (1982–2008). Journal of Geophysical Research: Biogeosciences, **116**.

Bindhu V, Narasimhan B, Sudheer K (2013) Development and verification of a non-linear disaggregation method (NL-DisTrad) to downscale MODIS land surface temperature to the spatial scale of Landsat thermal data to estimate evapotranspiration. Remote Sensing of Environment, **135**, 118-129.

Bjerke JW, Karlsen SR, Høgda KA *et al.* (2014) Record-low primary productivity and high plant damage in the Nordic Arctic Region in 2012 caused by multiple weather events and pest outbreaks. Environmental Research Letters, **9**, 084006.

Browning DM, Spiegal S, Estell RE, Cibils AF, Peinetti RH (2018) Integrating space and time: a case for phenological context in grazing studies and management. Frontiers of Agricultural Science and Engineering, **5**, 44-56.

Burrell AL, Evans JP, Liu Y (2018) The impact of dataset selection on land degradation assessment. ISPRS Journal of Photogrammetry and Remote Sensing, 146, 22-37.

de Beurs KM, Henebry GM (2004) Trend analysis of the Pathfinder AVHRR Land (PAL) NDVI data for the deserts of Central Asia. IEEE Geoscience and Remote Sensing Letters, **1**, 282-286.

de Beurs KM, Henebry GM, Owsley BC, Sokolik I (2015) Using multiple remote sensing perspectives to identify and attribute land surface dynamics in Central Asia 2001–2013. Remote Sensing of Environment, **170**, 48-61.

de Beurs KM, Henebry GM, Owsley BC, Sokolik IN (2018) Large scale climate oscillation impacts on temperature, precipitation and land surface phenology in Central Asia. Environmental Research Letters, **13**, 065018.

de Beurs KM, Wright CK, Henebry GM (2009) Dual scale trend analysis for evaluating climatic and anthropogenic effects on the vegetated land surface in Russia and Kazakhstan. Environmental Research Letters, **4**, 045012.

de Jong R, De Bruin S, De Wit A, Schaepman ME, Dent DL (2011) Analysis of monotonic greening and browning trends from global NDVI time-series. Remote Sensing of Environment, **115**, 692-702.

de Jong R, Verbesselt J, Schaepman ME, De Bruin S (2012) Trend changes in global greening and browning: contribution of short-term trends to longer-term change. Global Change Biology, **18**, 642-655.

Detsch F, Otte I, Appelhans T, Nauss T (2016) A comparative study of cross-product NDVI dynamics in the Kilimanjaro region—A matter of sensor, degradation calibration, and significance. Remote Sensing, **8**, 159.

Didan K, Munoz A, Solano R, Huete A (2015) MODIS vegetation index user's guide (MOD13 Series) version 3.00 (Collection 6). Vegetation Index and Phenology Lab. The University of Arizona, 1-38.

Duan S, Li Z, Cheng J, Leng P (2017) Cross-satellite comparison of operational land surface temperature products derived from MODIS Aster data over bare soil surfaces. ISPRS Journal of Photogrammetry and Remote Sensing, 126, 1-10.

Duan S, Li Z, Wu H, Leng P, Gao M, Wang C (2018) Radiance-based validation of land surface temperature products derived from Collection 6 MODIS thermal infrared data. International Journal of Applied Earth Observation and Geoinformation, 70, 84-92.

Duan S, Li Z, Li H, Gottsche F, Wu H, Zhao W, Leng P, Zhang X, Coll C (2019) Validation of Collection 6 MODIS land surface temperature product using in situ measurements. Remote Sensing of Environment, 225, 16-29.

Fan X, Liu Y (2016) A global study of NDVI difference among moderate-resolution satellite sensors. ISPRS Journal of Photogrammetry and Remote Sensing, 121, 177-191.

Fang X, Zhu Q, Ren L, Chen H, Wang K, Peng C (2018) Large-scale detection of vegetation dynamics and their potential drivers using MODIS images and BFAST: A case study in Quebec, Canada. Remote Sensing of Environment*,* **206**, 391-402.

Fensholt R, Proud SR (2012) Evaluation of earth observation based global long term vegetation trends—Comparing GIMMS and MODIS global NDVI time series. Remote Sensing of Environment*,* **119**, 131-147.

Fu P, Weng Q (2018) Variability in annual temperature cycle in the urban areas of the United States as revealed by MODIS imagery. ISPRS Journal of Photogrammetry and Remote Sensing, 146, 65-73.

Guay KC, Beck PS, Berner LT, Goetz SJ, Baccini A, Buermann W (2014) Vegetation productivity patterns at high northern latitudes: a multi-sensor satellite data assessment. Global Change Biology, **20**, 3147-3158.

Jiang C, Ryu Y, Fang H, Myneni R, Claverie M, Zhu Z (2017) Inconsistencies of interannual variability and trends in long-term satellite leaf area index products. Global Change Biology, **23**, 4133-4146.

Krehbiel C, Henebry GM (2016) A comparison of multiple datasets for monitoring thermal time in urban areas over the US Upper Midwest. Remote Sensing, **8**, 297.

Krehbiel C, Zhang X, Henebry GM (2017) Impacts of Thermal Time on Land Surface Phenology in Urban Areas. Remote Sensing, **9**, 499.

Lloyd AH, Bunn AG (2007) Responses of the circumpolar boreal forest to 20th century climate variability. Environmental Research Letters, **2**, 045013.

Lyapustin A, Wang Y, Xiong X *et al.* (2014) Scientific impact of MODIS C5 calibration degradation and C6+ improvements. Atmospheric Measurement Techniques, **7**, 4353-4365.

Murthy K, Bagchi S (2018) Spatial patterns of long-term vegetation greening and browning are consistent across multiple scales: Implications for monitoring land degradation. Land Degradation & Development. **29**, 2485-2495.

Pan N, Feng X, Fu B, Wang S, Ji F, Pan S (2018) Increasing global vegetation browning hidden in overall vegetation greening: Insights from time-varying trends. Remote Sensing of Environment, **214**, 59-72.

Potter C (2018) Recovery Rates of Wetland Vegetation Greenness in Severely Burned Ecosystems of Alaska Derived from Satellite Image Analysis. Remote Sensing, **10**, 1456.

Schaaf CB (2018) MODIS User Guide V006.

Sulla-Menashe D, Friedl MA (2018) User Guide to Collection 6 MODIS Land Cover (MCD12Q1 and MCD12C1) Product. https://lpdaac.usgs.gov/sites/default/files/public/product_documentation/mcd12_user_guide_v6.pdf, LP DAAC.

Sulla-Menashe D, Woodcock CE, Friedl MA (2018) Canadian boreal forest greening and browning trends: an analysis of biogeographic patterns and the relative roles of disturbance versus climate drivers. Environmental Research Letters, **13**, 014007.

Verbyla D (2011) Browning boreal forests of western North America. Environmental Research Letters, **6**, 041003.

Viglizzo EF, Frank FC, Carreño LV *et al.* (2011) Ecological and environmental footprint of 50 years of agricultural expansion in Argentina. Global Change Biology, **17**, 959-973.

Walker J, De Beurs K, Henebry G (2015) Land surface phenology along urban to rural gradients in the US Great Plains. Remote Sensing of Environment, **165**, 42-52.

Wan Z (2008) New refinements and validation of the MODIS land-surface temperature/emissivity products. Remote Sensing of Environment, **112**, 59-74.

Wan Z (2014) New refinements and validation of the collection-6 MODIS land-surface temperature/emissivity product. Remote Sensing of Environment, **140**, 36-45.

Wang D, Morton D, Masek J *et al.* (2012) Impact of sensor degradation on the MODIS NDVI time series. Remote Sensing of Environment, **119**, 55-61.

Wang Z, Schaaf CB, Sun Q, Shuai Y, Román MO (2018) Capturing rapid land surface dynamics with Collection V006 MODIS BRDF/NBAR/Albedo (MCD43) products. Remote Sensing of Environment, **207**, 50-64.

Wildlife Conservation Society - WCS, Center for International Earth Science Information Network - Ciesin - Columbia University (2005) Last of the Wild Project, Version 2, 2005 (LWP-2):

Global Human Influence Index (HII) Dataset (Geographic). Palisades, NY, NASA Socioeconomic Data and Applications Center (SEDAC).

Williamson SN, Hik DS, Gamon JA, Jarosch AH, Anslow FS, Clarke GK, Rupp TS (2017) Spring and summer monthly MODIS LST is inherently biased compared to air temperature in snow covered sub-Arctic mountains. Remote Sensing of Environment, **189**, 14-24.

Wongsai N, Wongsai S, Huete AR (2017) Annual Seasonality Extraction Using the Cubic Spline Function and Decadal Trend in Temporal Daytime MODIS LST Data. Remote Sensing, **9**, 1254.

Xiong X, Esposito JA, Sun J-Q, Pan C, Guenther BW, Barnes WL (2001) Degradation of MODIS optics and its reflective solar bands calibration. In: *Sensors, Systems, and Next-Generation Satellites V*.International Society for Optics and Photonics, 4540, 62-71.

Xu X, Piao S, Wang X, Chen A, Ciais P, Myneni RB (2012) Spatio-temporal patterns of the area experiencing negative vegetation growth anomalies in China over the last three decades. Environmental Research Letters, **7**, 035701.

Zhang H, Roy DP (2016) Landsat 5 Thematic Mapper reflectance and NDVI 27-year time series inconsistencies due to satellite orbit change. Remote Sensing of Environment, **186**, 217-233.

Zhang Y, Song C, Band LE, Sun G, Li J (2017) Reanalysis of global terrestrial vegetation trends from MODIS products: Browning or greening? Remote Sensing of Environment, **191**, 145-155.

Chapter 3: An Evaluation of the Archive Continuation of MODIS with VIIRS and the Data Consistency with Landsat for Data Fusion Techniques

Abstract

The launch of Landsat in 1972 and MODIS in 1999 has provided the remote sensing community with two uninterrupted and relatively stable data archives that can be used to evaluate land surface change over time. Archive continuation through succeeding missions is highly important in preserving and creating deep repositories of information for Earth observation, which has been done with the Landsat data continuity mission. However, with varying spectral and spatial resolution, it can be a challenge to harmoniously continue archives through different platforms such as planned with MODIS and VIIRS. In this study, I evaluate the consistency of Landsat, MODIS, and VIIRS to evaluate how these data streams can be used in data fusion and in the continuation of the MODIS archive with VIIRS. The surface reflectance from Landsat, the MYD09GA and MCD43A4 products from MODIS, as well as the VNP09GA and VNP43IA4 products from VIIRS, are used to carry out the analysis. In addition to surface reflectance, the products are also evaluated through NDVI. I conduct this analysis on the north island of New Zealand, the multiple land covers and their fragmented tendencies will best represent how well the sensors correlate in a potentially complex land surface scenario.

1. Introduction

Understanding global and regional land use and land cover change has become increasingly relevant due to climate change and expanding urban environments. Specifically, examining the disturbances of biomes such as forests and grasslands may become a vital step in managing and understanding our changing climate because of their key involvement in the carbon cycle. Forests and grasslands are significant terrestrial carbon stocks, as well as contributors to climate change mitigation, through carbon sequestration (O'Mara 2012; Hansen et al. 2013). Land-use change related contributions of carbon to the atmosphere has accounted for a cumulative quarter of emissions since industrialization (Song et al., 2018). Providing information about forest disturbance can be key in policy and management strategy for conservation of environments and their biodiversity but often has been poorly quantified (Hansen et al. 2013; Masek et al. 2008). However, the global forest cover loss continues to be significant: from 2001 – 2015 there was a 3.14 million km^2 of loss globally with the greatest drivers of loss, in order from greatest to least, being forestry (31%), deforestation (25%), wildfire (22%), shifting agriculture (22%), and urbanization (<1%) (Curtis et al., 2018). However, between 1982 and 2016 there has also been a 2.24 million km^2 increase in tree cover. This gain can be explained by a net loss in the tropics with an overwhelming net gain in the subtropical, temperate and boreal climate zones (Song et al., 2018). Likewise, grasslands have experienced degradation but have received significantly less attention in comparison to other production systems (Bengtsson et al., 2019). Globally about 3.2 billion people live in degrading areas, which include croplands, forests, shrubland, and grassland. With 33% of grasslands experiencing a human induced decline of biomass productivity, many people could be affected directly or indirectly through the disturbance of ecosystem goods and services (Nkonya et al., 2016).

The ideal strategy for monitoring change in forests and grasslands is a time series of satellite images. Time series data from satellite observations give researchers the ability to learn from past occurrences, monitor current conditions, and potentially prepare for future events. Analyzing historical data will contribute to our forecasting ability and making inferences about changing climate conditions (van Leeuwen et al. 2006). However, to perform this type of analysis, consistent long-standing archives need to be available. Fortunately, the research community has sensors such as Landsat and MODIS (MODerate Imaging Spectroradiometer) that have been collecting data since 1972 and 2000, respectively. Landsat data have been available semi-continuous since 1972 with the launch of eight missions. Landsat 9 is slated to be launched in 2021. The MODIS sensors are aboard the two satellites Terra and Aqua launched in 1999 and 2002, they provide individual and combined products.

1.1 Importance of continuous archives

Using remotely sensed data is the only feasible way of monitoring change on a relatively large scale. Landsat has often been the source for providing regional analysis because of its spatial scale and continuous observations (Healey et al. 2005). However, Landsat can be challenging to use for change analysis because of its low temporal resolution and the visual obstruction from clouds. Landsat collects an image over a single area once about every sixteen days but there is no guarantee this image will be of good quality, potentially making it difficult to put together a consistent time series. However, sensors with coarser spatial resolution, such as MODIS, have a much higher temporal resolution of one day. Additionally, there are MODIS derived products that are formed through compositing that provide cloud free images. This temporal strength, unfortunately, comes at the cost of spatial resolution, as MODIS products are offered at resolutions of 250, 500, 1000, and 5600 meters, while Landsat is 30 meters. Each

sensor provides its own distinct advantage that researchers must consider when designing their research plan.

The existence and use of continuous data archives in time series analysis will continue to be extremely relevant for monitoring our changing landscapes. Unfortunately, sensors, like everything else, degrade and can start to produce erroneous results. While the sensor's sensitivity can degrade overtime, on board calibration equipment for sensors such as MODIS and VIIRS can also degrade. In addition to gradual decline, specific events can initiate or accelerate degradation. This was the case with MODIS Terra where a pre-launch event caused significant degradation (Lyapustin et al. 2014). The Landsat archive has been successful in uninterrupted observations because of the periodic launch of new satellites. The MODIS sensors aboard Terra and Aqua, like Landsat, have been extremely relevant in Earth science studies. However, the MODIS sensor aboard Terra has already begun to experience degradation (Skakun et al. 2018; Heck et al. 2019). As the MODIS sensors continue to operate past their design life, it is important to establish the successor and its consistency with the current archives. The data continuity of MODIS will be obtained through using VIIRS (Visible Infrared Imaging Radiometer Suite) flying on the converged National Polar-Orbiting Environmental Satellite System (NPOESS) and on the NPOESS Preparatory Project (Murphy et al. 2001). Skakun et al. (2018), evaluated the performance of MODIS and VIIRS by quantifying uncertainty at near nadir observations through agricultural monitoring using NDVI. They found that the uncertainty was low for same day and close to nadir observations for daily and composited product.

1.2 Similarities and differences between MODIS and VIIRS equipment and collection

The moderate resolution data archive produced by the MODIS sensors aboard the Terra and Aqua platforms since their launch in the early 2000's has resulted in many widely applicable

products that serve a range of disciplines in biology, atmospheric science, climatology, and land change. The development and launch of VIIRS will continue the legacy of regional and continental scale studies for which MODIS has provided a platform for nearly twenty years. As the planned successor, VIIRS is comparable to MODIS in all major interests such as spatial, spectral, temporal, and radiometric resolution. Differences do exist between the two platforms resolutions but the varying specifics between the instruments have been intentionally designed for data product continuity. In addition to the similarities between data collection, the on-board calibration equipment is also nearly identical, with both sensors using a single black body source, a solar diffuser, and solar diffuser stability monitor (Murphy et al., 2001). However, it has been documented that the equipment aboard MODIS Terra has experienced significant degradation due to a pre-launch event (Lyapustin et al., 2014). This degradation highlights the importance of understanding of how the scientific community will transition between data sources, therefore, we must better understand the consistency among the MODIS and VIIRS sensors (Skakun et al., 2018; Villaescusa-Nadal et al., 2019).

Although VIIRS is designed to be the successor to MODIS, the sensor design has several differences that impact archive continuity. The Aqua MODIS sensor is more similar to VIIRS than Terra because of close acquisition times. However, the MODIS MCD products are generated by combining Terra and Aqua data, potentially negatively impacting the correlation of VIIRS and MODIS data collected at the same time. While the algorithms to calculate surface reflectance between VIIRS and MODIS are similar, the fundamental spectral, angular, and spatial differences between the instruments are expected to cause differences between the data streams (Liu et al., 2017). The solar and viewing geometries of VIIRS and MODIS are similar, but not identical. MODIS has a swath width of 2330km while VIIRS has a larger swath of 3040km. The MODIS gridded product footprint is ~500m at nadir, but as the degree off nadir

increases the pixel footprints also increase, once the sensor is 55° off nadir the footprint is >3000m. As mentioned before, VIIRS collects its I (375m) and M (750m) bands at different resolutions and the data are later aggregated to 500 and 1000 meters to be consistent with current MODIS products. The gridded product for VIIRS is collected at its two resolutions at nadir and similarly grow as the degree off nadir increases. However, VIIRS utilizes on-board processing that limits pixel growth through aggregation of sub-pixels (Liu et al., 2017). These differences between the underlying footprints in VIIRS and MODIS cause the effective spatial resolution to differ significantly. The MODIS effective resolution at mid latitudes for the 500m NBAR product is approximately 833x618m while VIIRS is approximated at 565x595m (Liu et al., 2017). Therefore, while the delivered products are aggregated to coinciding MODIS products for continuity, it is collection differences such as this that should be considered in partnering these data sources.

However, there have been several works assessing the bias and consistency between MODIS and VIIRS (Skakun et al., 2018; Uprety et al., 2013). A greater quantified understanding of how the spectral resolution, spatial resolution, and calibration differences effect coinciding results from MODIS and VIIRS will allow for the integration of VIIRS into current MODIS applications (Skakun et al., 2018). Liu et al. (2017) found that when comparing the NBAR values across multiple land covers at various latitudes, that VIIRS demonstrated a small positive bias but overall only had an absolute bias <0.013. The results yielded accuracy requirements needed by climate modelers and therefore, it was concluded that VIIRS provides a continuous, high-quality product that can be used by global and regional modelers. Skakun et al. (2018) also evaluated the uncertainty between MODIS and VIIRS red and NIR reflectance and NDVI in the daily and 8-day composite surface reflectance. They observed that the uncertainties were 0.014, 0.029, 0.056 for red, NIR, and NDVI, respectively, for the same-day daily reflectance product.

However, when comparing the 8-day composite data, the observation is constructed by 'best-pixels' within the 8-day window. The greater temporal range in observations caused there to be a 14% increase in uncertainties.

The aforementioned works contribute to the understanding of MODIS and VIIRS archive continuity in heterogeneous landscapes. It is pertinent to evaluate how the sensor platforms correlate beyond studies of calibration points. Additionally, the consistency between composited products need to be evaluated along with daily surface reflectance. In the case of Skakun et al. (2018), as expected, the uncertainties increase when comparing composited products in comparison to daily products. However, these studies do not explain the performance across land cover type. Depending on the application, it is imperative to understand correlation in grassland vs correlation in forests, for example. Challenges to collecting consistent measurements from multiple platforms may be particularly increased when routine disturbances are introduced to the landscape.

1.3 Landsat and data fusion

The continued Landsat archive and extended NDVI record through AVHRR and MODIS have set a model of consistency for the VIIRS program. In addition to consistent archives, there is also interest in fusing satellite datasets to leverage the advantageous characteristics of different platforms. However, combining different sensors, especially those that have vastly different spatial resolutions, pose several conceptual and technical challenges such as the orbital, spectral, and spatial configurations. The measured physical values are affected as a consequence (Mandanici and Bitelli, 2016). Although sensors may have contrasting spatial and spectral resolutions, it has been demonstrated these different data streams can be used for data fusion

(Gao et al., 2010), and can give greater access to unobstructed scenes, or multiple options for archive continuity (Mandanici and Bitelli, 2016).

There are several techniques for fusing data products so that the stronger temporal and spatial resolution of each product can be used to create more frequent observations of high-resolution data. The spatial and temporal adaptive reflectance fusion model (STARFM) was established to predict daily surface reflectance at Landsat spatial resolution using the daily revisit time of MODIS (Gao et al., 2006). Building on STARFM, the enhanced STARFM (ESTARFM) was created to overcome the limitations of the STARFM in heterogeneous landscapes. It improves on the original algorithm by using the observed reflectance trend between two points in time and spectral unmixing theory (Zhu et al., 2010). The ability of the algorithms to predict surface reflectance by using two data sources helps overcome limitations created by visual obstruction or infrequent observations. This can be applied, for example, in phenological studies where the spatial and temporal resolution of a single sensor is insufficient. In an effort to track phenological changes in dryland forests Walker et al. (2012), found that the synthetic high-resolution imagery that the STARFM algorithm produces can be valuable asset in analyzing dryland vegetation.

Therefore, going forward it will be important to continue data fusion application beyond the operational life of MODIS. The correlation between MODIS and Landsat allows for the successful fusion between the two sensors. Consequentially, I explore the relationship between Landsat and VIIRS to generate a greater understanding if the two platforms could be candidates for fusion. The relationship between VIIRS and Landsat will determine if it is feasible to assume there could be future fusion approaches developed to accommodate the pairing of VIIRS and Landsat.

1.4 Study Contributions

In this thesis, I am to provide a better understanding of the consistency of MODIS and VIIRS across four land cover types in a heterogeneous and fragmented landscape in the North Island of New Zealand. Additionally, I evaluate the consistency of Landsat 8 OLI measurements with coinciding MODIS and VIIRS data in the interest of data fusion that is currently performed with MODIS and Landsat and in the future may rely on VIIRS for continued application. I evaluate the consistency of theses sensors through red, NIR, NDVI, and tasseled cap transformation measurements. It is common to evaluate sensor consistency through red and NIR reflectance, NDVI, and albedo. In this work, I also incorporate the use of the Tasseled Cap Transformations (Crist, 1985; Kauth and Thomas, 1976) (TCT) of brightness, greenness, and wetness. The TCT performs a data reduction of seven (MODIS) or six (Landsat) surface reflectance bands into the three aforementioned physical characteristics. The TCT enables the evaluation of sensor performance from information derived through multiple bands, covering a broader range of the electromagnetic spectrum. Since the TCT provides information about physical characteristics about the terrestrial surface, we gain a greater understanding of how surface dynamics can play a role in sensor performance. Also, this study frames these relationships in practical terms, using a heterogenous landscape and not quasi-stable calibration sites.

2. Study Area

The study region is located centrally on the North Island of New Zealand (Figure 16), extending west beyond Lake Taupo and the eastern boundary being in Hawke Bay. The two primary landcover types in the North Island of New Zealand are forests and grasslands. As of 2012, 32% of New Zealand's land cover was indigenous forest, and 12% was considered plantation forests. Grasslands covered almost 50% of the North Island, with 3.5% classified as

low-producing grasslands, and 46% of the land area converted to high-producing grasslands, which are heavily grazed and often irrigated (de Beurs et al. 2016). Exotic forests include types of pine, Douglass fir, or evergreen broadleaf species. Indigenous forest is a less specific class of forest demarcated by vegetation dominated by tall forest canopy species. The lumber harvesting in the exotic class can have large section of cleared forest, adding to the variability of observations. High producing grasslands are typically exotic species of grasses that are intensively managed with irrigation and fertilizer for the purposes of intense grazing. Low producing grassland can be comprised of exotic and indigenous species and are indicated by having low plant vigor and biomass in comparison to the high producing class.

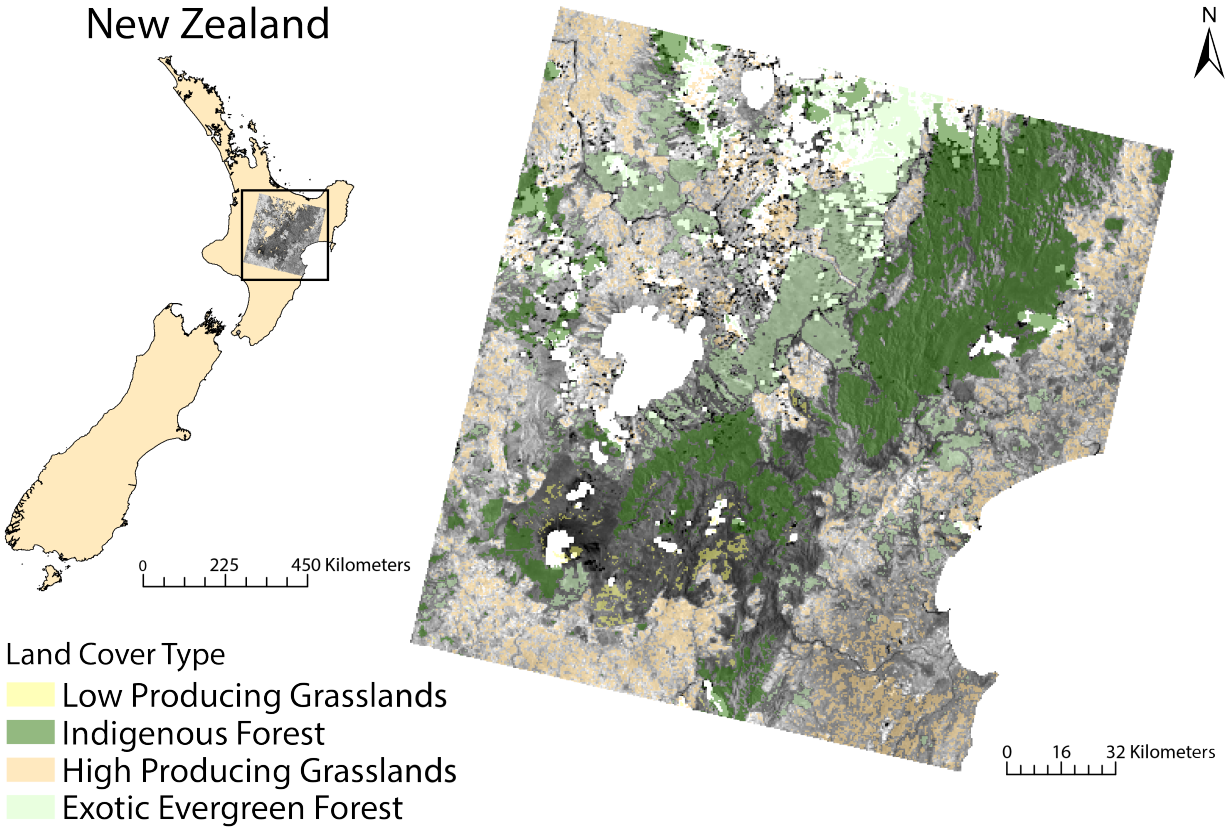

Figure 16. The location of the study area is displayed with the Landsat image that was used in the analysis. It is accompanied by the land cover classes evaluated and shows the cloud and water masked in white areas.

3. Data

To evaluate the consistency between the MODIS and VIIRS sensors, the surface reflectance and the NBAR products were compared for four major landcover types: indigenous forest, exotic evergreen forest, low producing grassland, and low producing grassland. Random samples from each class were derived from the New Zealand Land Cover Database (LCDB). The LCDB is a dataset produced by the Ministry for the Environment, Ministry of Agriculture and Forestry, and the Department of Conservation in New Zealand. The surface reflectance from Landsat 8 OLI was also compared against the MODIS and VIIRS surface reflectance to assess the feasibility of partnering VIIRS and Landsat data. The MODIS NBAR product is a combined product that utilizes observations from both Terra and Aqua satellites. However, I have elected to use surface reflectance from Aqua to compare with VIIRS because it has more similar orbital parameters with VIIRS, having an afternoon equatorial crossing time of about 1:30pm. Additionally, Terra has experienced significant degradation.

The Moderate Resolution Imaging Spectroradiometer (MODIS) is a near polar, sun-synchronous sensor aboard the two satellite platforms of Terra and Aqua of which were launched in 1999 and 2002, respectively. MODIS has a swath width of 2330km and spatial resolutions of 250m (bands 1-2), 500m (bands 3-7), and 1000m (bands 8-36). Having two platforms, Terra with a morning equatorial crossing time and Aqua crossing locally in the afternoon, the chances of having quality unobstructed images that benefit land, ocean, and atmospheric studies are increased. Using both platforms combined, a composited data product can be created that exploits the full range of the systems advantages. Additionally, this also allows for cross-calibration, which has revealed advanced degradation in the Terra sensor in comparison to Aqua. MODIS is used in many scientific communities because of its strong temporal capabilities, long standing archive, and wide spectral range.

The Visible Infrared Imaging Radiometer Suite (VIIRS) is also a near polar, sun-synchronous sensor. VIIRS is aboard the Suomi National Polar-orbiting Partnership (S-NPP) satellite that is the first in a series of five VIIRS instruments to be deployed in a collaborative effort between NOAA and NASA. VIIRS is a whisk broom sensor like MODIS but has a ~700km wider swath. This larger swath ensures that there are no data gaps near the equator. VIIRS is the designed successor that is expected to continue the moderate resolution surface observations currently established by originally by AVHRR and since 2000 by the MODIS sensor. VIIRS collects its observations at a resolution of 375m (I Bands 1-5) and 750m (M bands 1-16) but in the interest of archive continuation, the data is resampled to 500m, 1km, and 0.05 degrees in order to be cohesive with the existing data products of MODIS.

To compare the three platforms, I use coinciding daily surface reflectance and a composited NBAR product. From those data products the red, NIR, and NDVI are used to explore the relationship between sensors. Daily surface reflectance is used because theoretically, it is a physical measurement that is corrected for atmospheric effects and not affected by sensor calibration issues (Gao et al., 2010). It is advantageous to assess the consistency of the NBAR products because of their widespread application in interests such as vegetation phenology, land surface patterns, and photosynthetic activity but also because they are unaffected by the effects of satellite view angle (Liu et al., 2017). The NBAR is a nadir BRDF adjusted reflectance product that creates a nadir image formed by a composite of observations. The BRDF corrects the effects caused by viewing and illumination geometry. The quality information provided with the MODIS, VIIRS, and Landsat was used to filter out cloud shadows and low quality observations.

For MODIS and VIIRS I compared the daily surface reflectance and a composited NBAR product. The MODIS version 6 Nadir Bidirectional Reflectance Distribution Function (BRDF)-

Adjusted reflectance (NBAR) product (MCD43A4) is produced daily, using 16 days of observations at 500m spatial resolution. This product creates a nadir reflectance for bands 1-7, removing the sensor view angle effects and is temporally weighted to the ninth day. The MODIS daily reflectance product (MYD09GA) is derived from MODIS Aqua and is an estimate of surface reflectance delivered daily at 500m spatial resolution. The surface reflectance algorithm corrects for atmospheric conditions for bands 1-7. The VIIRS NBAR product (VNP43IA4) is delivered at 500m resolution and is produced to promote the continuity of the MODIS NBAR product. Similarly to MODIS, this product is produced daily using 16 days of observations and is weighted temporally to the ninth day. The product provides a nadir observation for bands I1 (600 – 680nm), I2 (850 – 880nm), and I3 (1580 – 1640nm). VIIRS daily estimate of surface reflectance (VNP09GA) is delivered at 500m for bands I1-I3 and 1 kilometer for bands M1-M5, M7, M8, M10, M11. The 500m data used in this study is resampled from the native 375m resolution of VIIRS. The Landsat 8 OLI is corrected to surface reflectance and is acquired at 30m spatial resolution. There is a temporal repeat cycle about every 16 days.

Table 9: The table shows the datasets used and their collection dates.

Sensor	Product Name	Location	Date
MODIS	MCD43A4	h31v12	01/23/2016 (center of composite)
MODIS	MYD09GA	h31v12	01/23/2016
VIIRS	VNP43IA4	h31v12	01/23/2016 (center of composite)
VIIRS	VNP09GA	h31v12	01/23/2016
Landsat 8 OLI	Surface Reflectance	Path: 72 Row:87	01/23/2016

4. Methods

To evaluate the consistency between VIIRS, MODIS, and Landsat, the red and NIR surface reflectance, as well as the NDVI was used to evaluate the correlation between data streams in

high producing grasslands, low producing grasslands, exotic evergreen forest, and indigenous forest. The data products were first filtered for clouds, cloud shadows and low-quality observation with quality bit or band information. The Landsat surface reflectance was aggregated to ~463 meters, the same size as the MODIS and VIIRS products. The Landsat data is resized to make comparison with the lower spatial resolution products of MODIS and VIIRS more reasonable. After aggregation, a one cell buffer was filtered out of the Landsat data to prevent cloud adjacent cells values from negatively impacting the aggregated data. The datasets were compared through random samples drawn from the land cover classification. The land cover classifications were determined by the New Zealand NLCD homogeneous pixels, where mixed pixels were not eligible to be drawn from for the sample of pixels compared for each class. For each of the land covers, except low producing grasslands, a random sample of 500 pixels was drawn. The number of pixels used in analysis varied across land cover type based on varying level of cloud obstruction and pixel quality. The sample drawn from the low producing grasslands were originally 300 pixels and then similarly filtered down due to cloud cover and quality issues. A smaller sample was drawn from low producing grasslands because the percentage of area occupied by low producing grasslands within the study area is only 0.63%. The same random sample was used to retrieve the red, NIR, NDVI, and TCT. The R^2 value, mean and standard deviation was calculated for each measurement to evaluate the linear relationship, variance, and how values from each sensor compared against one another.

5. Results

To evaluate the relationship between sensors, the red, NIR and NDVI were compared across four land cover types using the coefficient of determination, standard deviation, and mean values for each band. The measures of consistency and variation were calculated for the daily surface reflectance of MODIS, Landsat 8, and VIIRS. The composited NBAR products for

MODIS and VIIRS were compared against each other as well as the Landsat 8 daily surface reflectance.

Overall, by looking at figures 17 and 18 the coefficient of determination describing the linear relationships between the three sensors for the daily surface reflectance (figure 17) and modeled NBAR product (figure 18), it can be observed that the relationships vary by land cover and sensor combination. In figure 17, it can be seen that the grasslands consistently produce more quality relationships in comparison to the forests, especially for NDVI. While the NBAR product displays significant linear relationships among all three sensor combinations, the MODIS/Landsat relationships interestingly show the most R^2 values over 0.6. Among both data products the indigenous forest class performs the worst in R^2. However, greater variance in some of the forest samples and clustering of like observations negatively impact the linear relationships in forest classes. Figures 19 and 20 display the mean and standard deviation for the red, NIR, and NDVI. The means of each band separated by land cover show that, generally, the sensors compare well across land cover type.

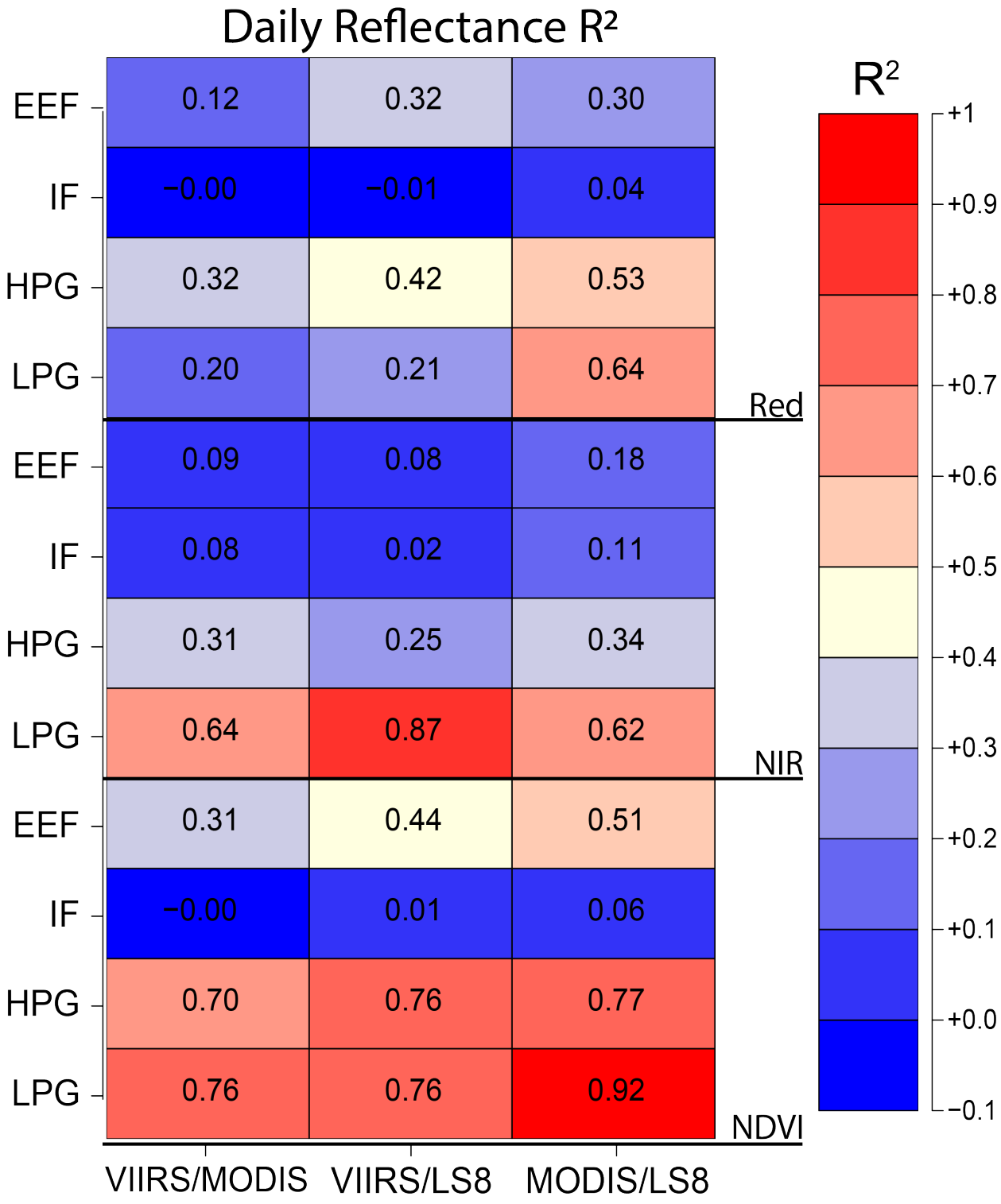

Figure 17. Daily Surface Reflectance grid of R^2 values between sensor relationships. Each row is representative of a land cover type of Exotic Evergreen Forest (EEF), Indigenous Forest (IF), High Producing Grassland (HPG), and Low Producing Grassland (LPG).

5.1 NDVI

The R^2 values for the daily surface reflectance for NDVI (figure 17) in the grasslands are greater than ~0.7, indicating a strong linear relationship. In contrast, the exotic forest ranges from ~0.3 – 0.5 and the indigenous forest never eclipses 0.1. All three of the sensor relationship combinations post similar results. Figure 19, showing the mean and standard deviation reveals that the exotic forest has the greatest standard deviations and the indigenous forest has the smallest. The mean for each sensor in the four different land covers are similar; however, consistently, the VIIRS mean is marginally highest while MODIS is the lowest. The NBAR NDVI (figure 18), similarly to the daily reflectance, performs well in the low producing grasslands but has a poorer performance in high producing grassland between VIIRS/MODIS (0.37) and VIIRS/LS8 (0.36). The VIIRS indigenous forest sample has the greatest standard deviation in the NBAR NDVI dataset. This is a vast difference in comparison to the coinciding Landsat and MODIS values, which have the smallest standard deviations.

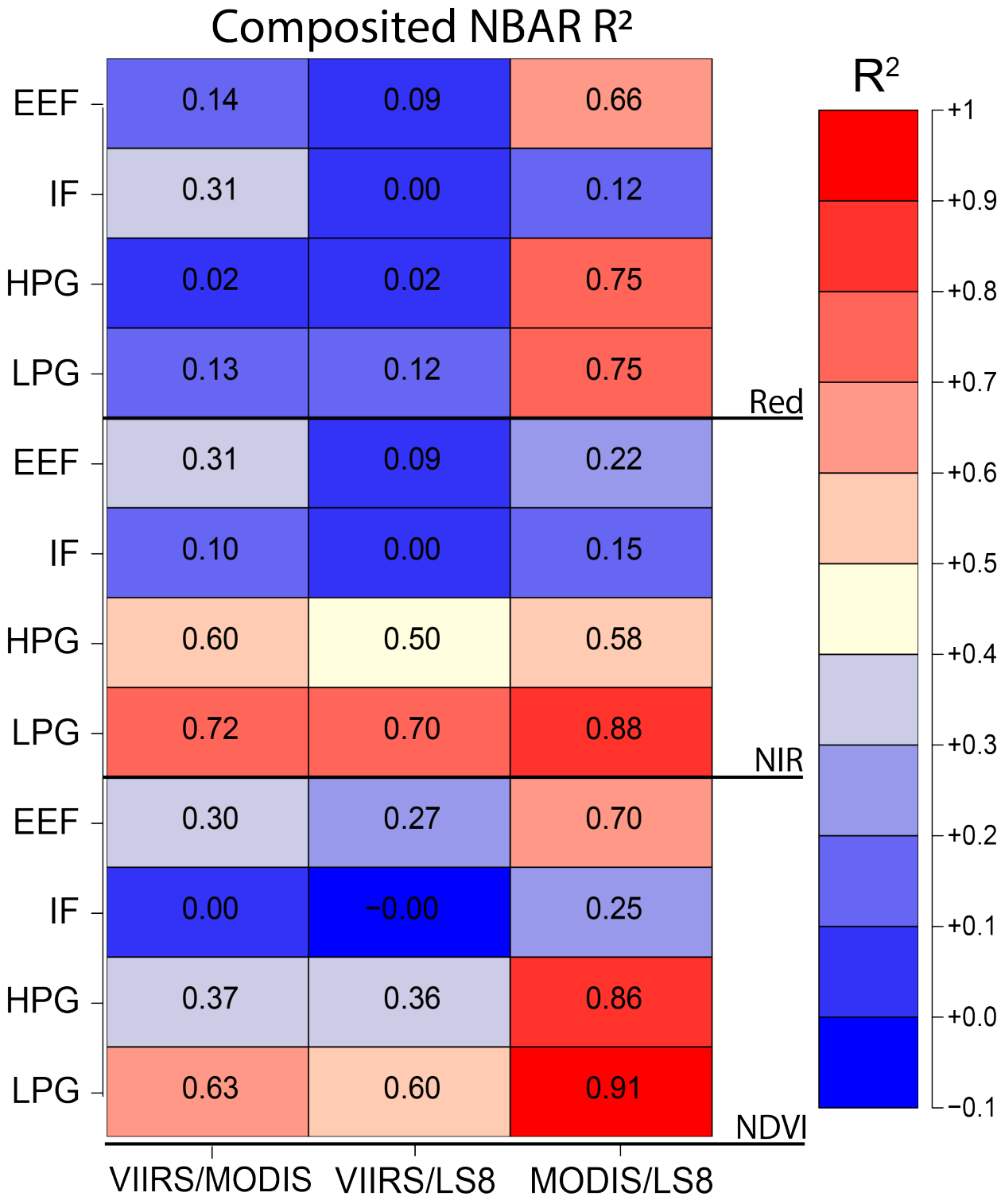

Figure 18. The figure represents a grid of R^2 values between sensor relationships for the Composited Nadir Bidirectional Reflectance Distribution Function (BRDF)-Adjusted Reflectance (NBAR) for MODIS and VIIRS compared against the daily Landsat image. Each row is representative of a land cover type of Exotic Evergreen Forest (EEF), Indigenous Forest (IF), High Producing Grassland (HPG), and Low Producing Grassland (LPG).

5.2 Red Reflectance

In figure 17, it can be seen that the two best R^2 values from the daily reflectance are in the MODIS/LS8 comparison in the low (0.64) and high (0.53) producing grasslands. The remaining grassland R^2 values range from 0.2 – 0.42. The indigenous forest performs poorest, not having an R^2 value exceed 0.04. Similarly, the exotic forest class does not produce a well performing linear relationship. Because the land cover types chosen in this study are vegetated areas, the red reflectance remains very low in all land cover types. The MODIS mean values for daily surface reflectance (figure 19) are consistently and marginally greater than Landsat and VIIRS observations. Similar to the NDVI, the greatest standard deviations are in the exotic forest samples, while the smallest are in the indigenous forest. Figure 18 similarly shows that there are few quality linear relationships in the composited NBAR red reflectance. However, three linear relationships exist between MODIS/LS8 in the exotic forest, high producing grassland, and low producing grassland are greater than 0.65. There are no relationships between VIIRS/MODIS and VIIRS/Landsat in the NBAR red reflectance that eclipse 0.31. Though the MODIS values in the daily reflectance (figure 19) were consistently highest, the VIIRS observations means are the highest in the NBAR product (figure 20). The standard deviations of the VIIRS observations are also greatest in all land cover types, especially in the indigenous forest.

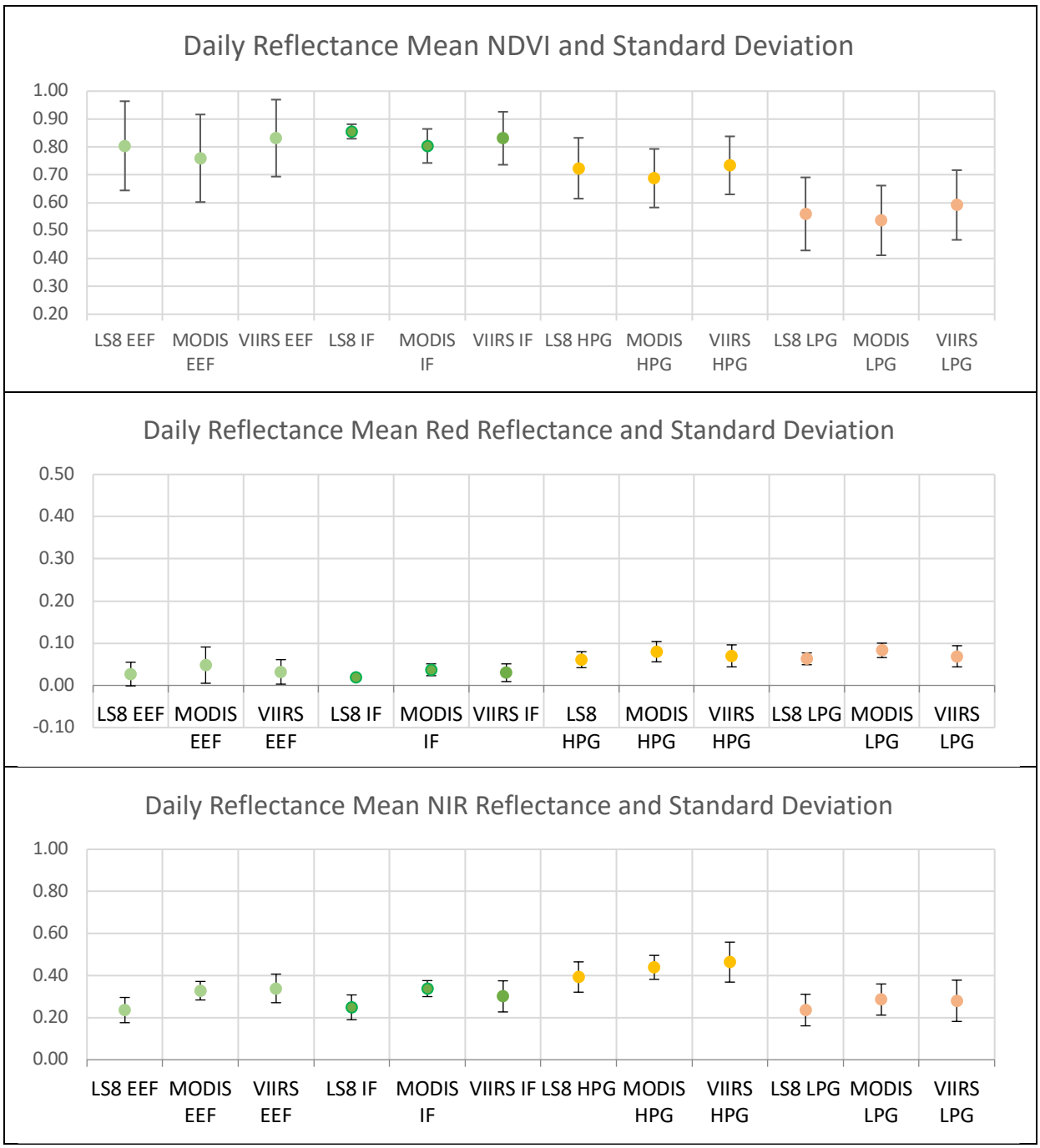

Figure 19. The three plots show the daily reflectance mean (points) and standard deviation (error bars) of NDVI, red, and NIR.

5.3 Near Infrared Reflectance

In the NIR daily reflectance, figure 17 displays a clear performance difference between forest and grasslands. Although both grassland classes do perform better than forests, the low

producing grasslands R^2 values are greater than 0.6. The forest R^2 values do not exceed 0.18 while the high producing grassland values range from 0.25 – 0.34. The mean values for the sensors in the four land cover types are similar but produce no consistent trend of one sensor producing greater means across all land cover types. The difference between R^2 performance in forest and grasslands are not as clear in the composited NBAR NIR reflectance in comparison to the daily reflectance. In the NBAR NIR reflectance, the low producing grasslands have the highest performance in the R^2 similarly to the daily reflectance with values ranging from 0.7 – 0.88. The high producing grasslands class has two moderately strong linear relationships between VIIRS/MODIS and MODIS/Landsat with values of 0.6 and 0.58, respectively.
The VIIRS observation means are the highest in all land cover types in the NBAR NIR reflectance while the Landsat means are the lowest. The standard deviations are similar across land cover types and the daily reflectance values.

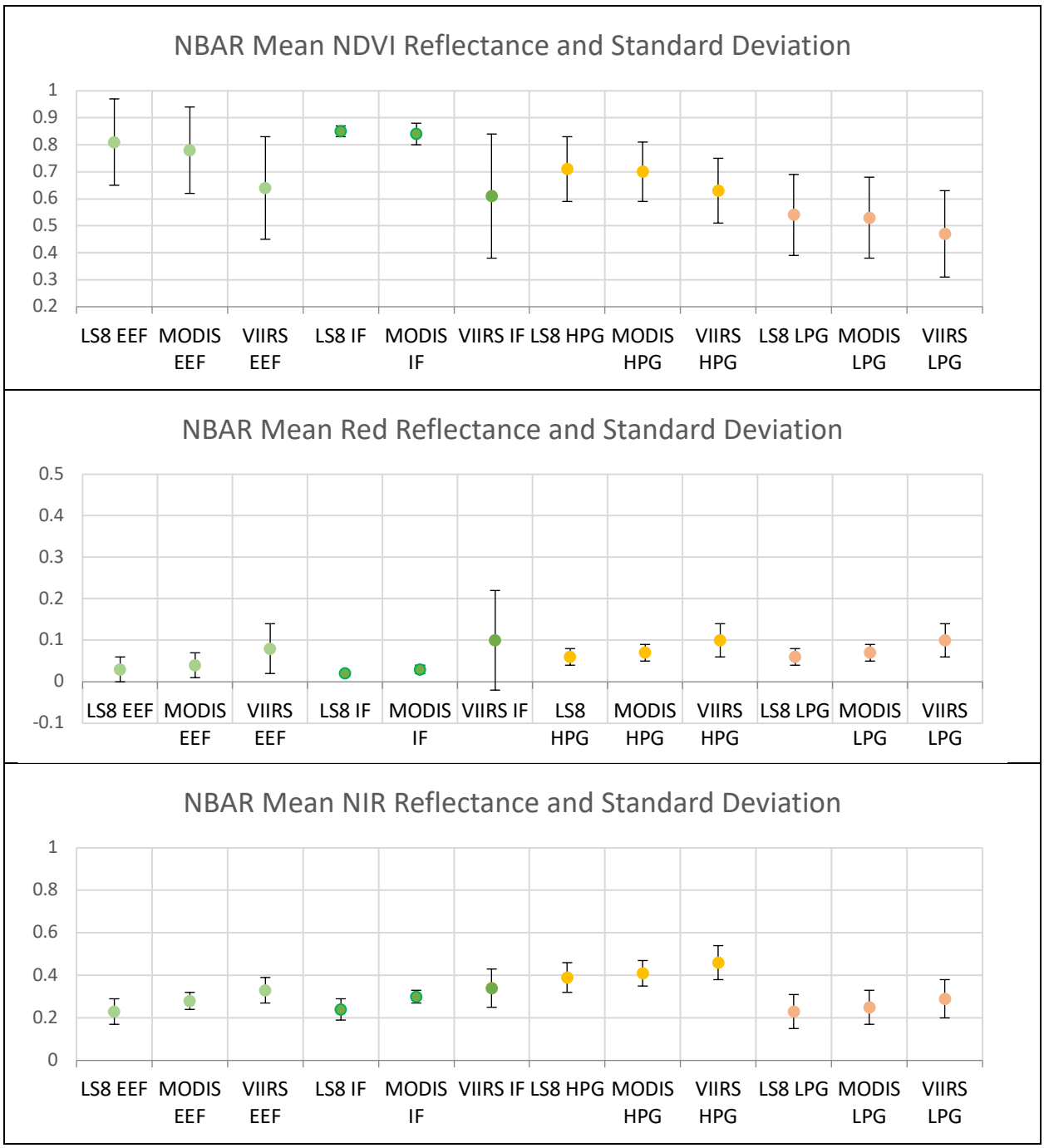

Figure 20. The three plots show the mean (points) and standard deviation (error bars) of NDVI, red, and NIR. The values for MODIS and VIIRS are derived from their respective NBAR products, while the Landsat data is from the daily image used throughout the analysis.

6. Discussion

The objective of this study can be looked at as two-fold. First, I was interested in assessing the continuity between the sensor platforms of MODIS and VIIRS. The NDVI record

established by AVHRR and continued with MODIS, in addition to MODIS products themselves, have generated multiple data products that have enabled researchers to evaluate 20+ years of change. As the MODIS sensors aboard Terra and Aqua age and degrade, especially in light of Terra's deteriorating performance, it will be paramount to transition to data provided by VIIRS. Due to VIIRS being the designated successor of the MODIS archive, thoughtful design and the creation of MODIS-like products will aid in combined use and transition. However, even though the VIIRS sensor was designed for MODIS continuity, the differences in sensor band width and viewing illumination geometries could make the two data streams correlate poorly (Gao et al., 2010). Therefore, to limit atmospheric and illumination differences, the observations are centered on or from the same day to minimize the differences in radiometry (Mandanici and Bitelli, 2016). Second, I evaluate the consistency of Landsat 8 surface reflectance with MODIS and VIIRS daily reflectance products and modeled composite NBAR products. The comparison of Landsat 8 and MODIS serves as a bench mark of performance because both platforms have been extensively validated. When MODIS data is no longer available it will become necessary to develop a similar partnership with VIIRS and Landsat.

To evaluate the agreement between the three sensors, the red and NIR surface reflectance as well as the NDVI was evaluated through the coefficient of determination, mean, and standard deviation. Overall, the best cross-sensor performance was found in the NDVI in grasslands. I also investigated the tasseled cap relationships (results not shown). The NDVI results were similar to the TCT of brightness greenness, and wetness between Landsat and MODIS. The low producing grasslands yielded R^2 values between 0.52 – 0.87 while the indigenous forest never had values greater than 0.13. It would be advantageous to evaluate the VIIRS data with the TCT because it would give greater insight to how VIIRS compares across multiple bands. However, the coefficients to calculate the TCT for VIIRS has not yet been established.

When evaluating sensor consistency by land cover, as done in this study, the data collected from a homogenous land cover type can create a cluster of data points rather than a linear relationship. The clustering of data points results in a poor coefficient of determination. The grasslands performed better than forest land cover types likely due the more simplified dynamics of collecting remotely sensed data from grasslands in comparison to forests. Similarly, (Liu et al., 2017) found that the homogeneity of grassland pixels produced relatively consistent phenological transition dates across spatial scales while mixed oak/grass savanna areas were less comparable. Forests have varying canopy height and more back ground interference. These findings are in accordance with (Gallo et al., 2005), who reported that forest classes returned low R^2 values when comparing MODIS and AVHRR. The indigenous forest class had the lowest performance in R^2 across both data products in red, NIR, and NDVI. In figures 19 and 20 it can be seen that indigenous forest has the smallest standard deviations outside of the VIIRS red band in the NBAR product. The greater standard deviation of VIIRS is in contrast to what is expected. The MODIS NBAR uses observations from both Terra and Aqua while the VIIRS NBAR only collects one observation per day. Therefore, a greater variability should be expected from the MODIS product. The large standard deviation in the VIIRS red band contributes to the large standard deviation in the NBAR NDVI as expected. The indigenous forest class has the smallest standard deviation because it is a relatively dense tree canopy that experiences few disturbances. In contrast to the exotic forest, which experiences significant disturbance from lumber harvesting. This type of disturbance changes the land cover type from forest to bare ground, grassland, or recovering forest growth depending on the temporal distance from the disturbance date and the observation. Disturbance and the stages of growth that follow will cause a greater range of values than the undisturbed forest, which can consequentially cause a better performing linear relationship. (Liu et al., 2017) found through evaluating the NBAR and narrow band

albedo of MODIS and VIIRS that the source provided comparable results and the accuracy requirement desired by climate modelers. We find that the differences in design and parameters can negatively impact the comparison of MODIS and VIIRS. Although they are comparable in some scenarios, land cover type should be considered in addition to adjustment. These findings are in accordance with (Brown et al., 2006), which found that there were land cover dependent differences when comparing a long term NDVI record between AVHRR and MODIS in tropical forests and high northern latitude Tundra.

To detect phenological changes or disturbance, it is necessary to have data with a high temporal resolution or spatial resolution, respectively. There have been successful applications of data fusion such as STARFM, proposed by (Gao et al., 2006) that have successfully paired the spatial advantages of Landsat and the temporal advantages of MODIS. An additional approach to data fusion can be the use of multiple sensors that are similar in spectral and spatial resolution. Since Landsat has a low temporal resolution, the difficulty to obtain an unobstructed image is compounded by the presence of clouds. However, if Landsat is paired with a source such as Sentinel, that is similar in spatial and spectral characteristics, the data can be used together. This technique of fusing data streams to obtain more consistent observations between Landsat and Sentinel can reduce the revisit time of 16 days to 5 days (Arekhi et al., 2019). If the degradation of MODIS Terra continues and advances the condition of the sensor to an unusable state, the VIIRS sensors could be used in conjunction with MODIS Aqua.

Although there are several systematic inconsistencies that limit ideal correlation without adjustment, the relationship with both MODIS/Landsat and VIIRS/Landsat has been evaluated. Landsat and MODIS have been extensively validated, it is important to consider their agreement as a reference for the performance between VIIRS/Landsat. In our R^2 results of red, NIR, and NDVI the comparative relationship between MODIS/Landsat performed best, even

outperforming the relationship between MODIS/VIIRS of which are designed for continuity and share more similar spatial characteristics.

Although sensors may vary in their intrinsic band width and viewing geometries, studies such as (Flood, 2017) show that comparable yet different platforms like Sentinel and Landsat 7 & 8 can compare well depending on the band in question. However, with spectral adjustment, the systematic difference between all bands can be less than one percent. There are three primary ways to perform spectral adjustment: band averaging, radiative transfer, and statistical regression (Villaescusa-Nadal et al., 2019). Through the use of ordinary least squares regression and four years of observations, Skakun et al. (2018) established coefficients to correct for the spectral bias between MODIS and VIIRS red and NIR bands. Using the coefficients, the uncertainty for the NDVI from MODIS/Aqua and VIIRS was <0.056 for near nadir and same day observations. Our results indicate that situationally, MODIS, VIIRS and Landsat can correlate well in grassland land covers, particularly when using NDVI. If these data sources are used together in forested regions, it is recommended that adjustment be applied. Identifying what causes differences between data streams can become complex due to varying calibration equipment, collection techniques, and product algorithms but discrepancies can be overcome by using error reducing techniques such as data smoothing and normalization (van Leeuwen et al. 2006).

This study makes valuable contributions to data continuity in respect to the continuation of the moderate resolution archive by comparing MODIS and VIIRS as well as evaluating the consistency of Landsat 8 and VIIRS in the case of future data fusion use. However, there are limitations to the findings of the work due to project scope and the nature of evaluating varying spatial, spectral, and temporal resolution datasets. First, the scope of this project only allowed analysis of four land cover types in the bounding area of one Landsat tile. Ideally, several tiles would have been evaluated in different environments. Additionally, a time series could be

evaluated so that the consistency between sensors could be temporally assessed as well as spatially. Even with these limitations in scope, our evaluation of sensor consistency between MODIS, VIIRS, and Landsat 8 across multiple land covers gives insight to how these datasets correlate in a fragmented and complex landscape in contrast to studies performed in quasi-stable calibration sites.

7. Conclusion

As mentioned earlier in the manuscript, the MODIS and VIIRS datasets, by design, are delivered in the same spatial resolution to enable product continuation. However, the collection and processing of the dataset have significant differences that will negatively impact their agreement. The native resolution and pixel growth as the off-nadir viewing angle increases (Liu et al., 2017) will fundamentally change the results of the remotely sensed terrestrial surface by the surface reflectance product. The modeled NBAR product consistency is negatively impacted by the previous factors as well as the nearly twice as many observations collected by MODIS on Terra and Aqua.

Additionally, the results indicate that the correlation of the sensors does depend on land cover type. The more simplified structure of grasslands leads to stronger relationships between sensors. The results suggest that if the datasets discussed here are used in conjunction, then adjustment should be applied, particularly in forested landscapes. Going forward, continued work should be done on cross-sensor performance in complex land surface scenarios rather that stable calibration points.

References

Arekhi, M., Goksel, C., Balik Sanli, F., Senel, G., 2019. Comparative Evaluation of the Spectral and Spatial Consistency of Sentinel-2 and Landsat-8 OLI Data for Igneada Longos Forest. IJGI 8, 56. https://doi.org/10.3390/ijgi8020056

Bengtsson, J., Bullock, J.M., Egoh, B., Everson, C., Everson, T., O'Connor, T., O'Farrell, P.J., Smith, H.G., Lindborg, R., 2019. Grasslands-more important for ecosystem services than you might think. Ecosphere 10, e02582. https://doi.org/10.1002/ecs2.2582

Brown, M.E., Pinzon, J.E., Didan, K., Morisette, J.T., Tucker, C.J., 2006. Evaluation of the consistency of long-term NDVI time series derived from AVHRR,SPOT-vegetation, SeaWiFS, MODIS, and Landsat ETM+ sensors. IEEE Transactions on Geoscience and Remote Sensing 44, 1787–1793. https://doi.org/10.1109/TGRS.2005.860205

Crist, E.P., 1985. A TM Tasseled Cap equivalent transformation for reflectance factor data. Remote Sensing of Environment 17, 301–306. https://doi.org/10.1016/0034-4257(85)90102-6

Curtis, P.G., Slay, C.M., Harris, N.L., Tyukavina, A., Hansen, M.C., 2018. Classifying drivers of global forest loss. Science 361, 1108–1111. https://doi.org/10.1126/science.aau3445

de Beurs, K.M., Owsley, B.C., Julian, J.P., 2016. Disturbance analyses of forests and grasslands with MODIS and Landsat in New Zealand. International Journal of Applied Earth Observation and Geoinformation 45, 42–54. https://doi.org/10.1016/j.jag.2015.10.009

Flood, N., 2017. Comparing Sentinel-2A and Landsat 7 and 8 Using Surface Reflectance over Australia. Remote Sensing 9, 659. https://doi.org/10.3390/rs9070659

Gallo, K., Ji, L., Reed, B., Dwyer, J., Eidenshink, J., 2004. Comparison of MODIS and AVHRR 16-day normalized difference vegetation index composite data: COMPARISON OF MODIS AND AVHRR DATA. Geophys. Res. Lett. 31, https://doi.org/10.1029/2003GL019385

Gallo, K., Ji, L., Reed, B., Eidenshink, J., Dwyer, J., 2005. Multi-platform comparisons of MODIS and AVHRR normalized difference vegetation index data. Remote Sensing of Environment 99, 221–231. https://doi.org/10.1016/j.rse.2005.08.014

Gao, F., Masek, J., Schwaller, M., Hall, F., 2006. On the blending of the Landsat and MODIS surface reflectance: predicting daily Landsat surface reflectance. IEEE Transactions on Geoscience and Remote Sensing 44, 2207–2218. https://doi.org/10.1109/TGRS.2006.872081

Gao, F., Masek, J.G., Wolfe, R.E., Huang, C., 2010. Building a consistent medium resolution satellite data set using moderate resolution imaging spectroradiometer products as reference. Journal of Applied Remote Sensing 4, 043526. https://doi.org/10.1117/1.3430002

Glenn, E., Huete, A., Nagler, P., Nelson, S., 2008. Relationship Between Remotely-sensed Vegetation Indices, Canopy Attributes and Plant Physiological Processes: What Vegetation Indices Can and Cannot Tell Us About the Landscape. Sensors 8, 2136–2160. https://doi.org/10.3390/s8042136

Hansen, M.C., Potapov, P.V., Moore, R., Hancher, M., Turubanova, S.A., Tyukavina, A., Thau, D., Stehman, S.V., Goetz, S.J., Loveland, T.R., Kommareddy, A., Egorov, A., Chini, L., Justice, C.O., Townshend, J.R.G., 2013. High-Resolution Global Maps of 21st-Century Forest Cover Change. Science 342, 850–853. https://doi.org/10.1126/science.1244693

Healey, S., Cohen, W., Zhiqiang, Y., Krankina, O., 2005. Comparison of Tasseled Cap-based Landsat data structures for use in forest disturbance detection. Remote Sensing of Environment 97, 301–310. https://doi.org/10.1016/j.rse.2005.05.009

Heck, E., de Beurs, K.M., Owsley, B.C., Henebry, G.M., 2019. Evaluation of the MODIS collections 5 and 6 for change analysis of vegetation and land surface temperature dynamics

in North and South America. ISPRS Journal of Photogrammetry and Remote Sensing 156, 121–134. https://doi.org/10.1016/j.isprsjprs.2019.07.011

Ji, L., Gallo, K., Eidenshink, J.C., Dwyer, J., 2008. Agreement evaluation of AVHRR and MODIS 16-day composite NDVI data sets. International Journal of Remote Sensing 29, 4839–4861. https://doi.org/10.1080/01431160801927194

Kauth, R.J., Thomas, G.S., 1976. The Tasselled Cap -- A Graphic Description of the Spectral-Temporal Development of Agricultural Crops as Seen by LANDSAT. IEEE 13.

Li, P., Jiang, L., Feng, Z., 2013. Cross-Comparison of Vegetation Indices Derived from Landsat-7 Enhanced Thematic Mapper Plus (ETM+) and Landsat-8 Operational Land Imager (OLI) Sensors. Remote Sensing 6, 310–329. https://doi.org/10.3390/rs6010310

Liu, Y., Hill, M.J., Zhang, X., Wang, Z., Richardson, A.D., Hufkens, K., Filippa, G., Baldocchi, D.D., Ma, S., Verfaillie, J., Schaaf, C.B., 2017a. Using data from Landsat, MODIS, VIIRS and PhenoCams to monitor the phenology of California oak/grass savanna and open grassland across spatial scales. Agricultural and Forest Meteorology 237–238, 311–325. https://doi.org/10.1016/j.agrformet.2017.02.026

Liu, Y., Wang, Z., Sun, Q., Erb, A.M., Li, Z., Schaaf, C.B., Zhang, X., Román, M.O., Scott, R.L., Zhang, Q., Novick, K.A., Syndonia Bret-Harte, M., Petroy, S., SanClements, M., 2017b. Evaluation of the VIIRS BRDF, Albedo and NBAR products suite and an assessment of continuity with the long term MODIS record. Remote Sensing of Environment 201, 256–274. https://doi.org/10.1016/j.rse.2017.09.020

Lyapustin, A., Wang, Y., Xiong, X., Meister, G., Platnick, S., Levy, R., Franz, B., Korkin, S., Hilker, T., Tucker, J., Hall, F., Sellers, P., Wu, A., Angal, A., 2014. Scientific impact of MODIS C5 calibration degradation and C6+ improvements. Atmos. Meas. Tech. 7, 4353–4365. https://doi.org/10.5194/amt-7-4353-2014

Mandanici, E., Bitelli, G., 2016. Preliminary Comparison of Sentinel-2 and Landsat 8 Imagery for a Combined Use. Remote Sensing 8, 1014. https://doi.org/10.3390/rs8121014

Masek, J.G., Huang, C., Wolfe, R., Cohen, W., Hall, F., Kutler, J., Nelson, P., 2008. North American forest disturbance mapped from a decadal Landsat record. Remote Sensing of Environment 112, 2914–2926. https://doi.org/10.1016/j.rse.2008.02.010

Murphy, R.E., Barnes, W.L., Lyapustin, A.I., Privette, J., Welsch, C., DeLuccia, F., Swenson, H., Schueler, C.F., Ardanuy, P.E., Kealy, P.S.M., 2001. Using VIIRS to provide data continuity with MODIS, in: IGARSS 2001. Scanning the Present and Resolving the Future. Proceedings. IEEE 2001 International Geoscience and Remote Sensing Symposium (Cat. No.01CH37217). Presented at the IGARSS 2001., pp. 1212–1214 vol.3. https://doi.org/10.1109/IGARSS.2001.976795

Nkonya, E., Mirzabaev, A., von Braun, J. (Eds.), 2016. Economics of Land Degradation and Improvement – A Global Assessment for Sustainable Development. Springer International Publishing, Cham. https://doi.org/10.1007/978-3-319-19168-3

O'Mara, F.P., 2012. The role of grasslands in food security and climate change. Annals of Botany 110, 1263–1270. https://doi.org/10.1093/aob/mcs209

Skakun, S., Justice, C.O., Vermote, E., Roger, J.-C., 2018. Transitioning from MODIS to VIIRS: an analysis of inter-consistency of NDVI data sets for agricultural monitoring. International Journal of Remote Sensing 39, 971–992. https://doi.org/10.1080/01431161.2017.1395970

Song, X.-P., Hansen, M.C., Stehman, S.V., Potapov, P.V., Tyukavina, A., Vermote, E.F., Townshend, J.R., 2018. Global land change from 1982 to 2016. Nature 560, 639–643. https://doi.org/10.1038/s41586-018-0411-9

Tucker, C.J., 1979. Red and Photographic Infrared l,lnear Combinations for Monitoring Vegetation. Remote Sensing of Environment 8, 127–150.

Uprety, S., Cao, C., Xiong, X., Blonski, S., Wu, A., Shao, X., 2013. Radiometric Intercomparison between *Suomi-NPP* VIIRS and *Aqua* MODIS Reflective Solar Bands Using Simultaneous Nadir Overpass in the Low Latitudes. J. Atmos. Oceanic Technol. 30, 2720–2736. https://doi.org/10.1175/JTECH-D-13-00071.1

van Leeuwen, W.J.D., Orr, B.J., Marsh, S.E., Herrmann, S.M., 2006. Multi-sensor NDVI data continuity: Uncertainties and implications for vegetation monitoring applications. Remote Sensing of Environment 100, 67–81. https://doi.org/10.1016/j.rse.2005.10.002

Villaescusa-Nadal, J.L., Franch, B., Roger, J.-C., Vermote, E.F., Skakun, S., Justice, C., 2019. Spectral Adjustment Model's Analysis and Application to Remote Sensing Data. IEEE J. Sel. Top. Appl. Earth Observations Remote Sensing 12, 961–972. https://doi.org/10.1109/JSTARS.2018.2890068

Walker, J.J., de Beurs, K.M., Wynne, R.H., Gao, F., 2012. Evaluation of Landsat and MODIS data fusion products for analysis of dryland forest phenology. Remote Sensing of Environment 117, 381–393. https://doi.org/10.1016/j.rse.2011.10.014

Zhu, X., Chen, J., Gao, F., Chen, X., Masek, J.G., 2010. An enhanced spatial and temporal adaptive reflectance fusion model for complex heterogeneous regions. Remote Sensing of Environment 114, 2610–2623. https://doi.org/10.1016/j.rse.2010.05.032

Chapter 4: Conclusion

The two preceding chapters highlight that creating reliable and consistent data archives from remotely sensed data can be a challenge due to sensor degradation, drift, equipment failure, and marginally different specifications to new sensors. It is vital to many research communities to have long standing consistent archives of satellite data because remotely sensed observations are the most feasible way to observe large spatial areas over a long period. These archives of satellite data have been and will continue to be an essential resource for those evaluating the changing climate and land use/cover change. Due to the importance of this topic, there are continuing research efforts to provide greater context to how the widely used data streams perform.

In Chapter 2, I described that there is a known difference between the Terra and Aqua MODIS sensors. A pre-launch event has caused more rapid degradation to the Terra sensor in comparison to its counterpart aboard Aqua. However, the new collection 6 calibration and algorithm improvements sought to remedy this issue by making the Terra sensor correlate better with the more stable Aqua sensor. In doing so, it is possible there was an overcompensation that lead to the presence of more greening in our results based on the EVI and NDVI. In contrast to the VI results, the LST remained stable through collection 5 and 6. Although we found significant differences between the collections, there was still broad concordance. Dependent upon spatial location, the results indicate that users should be aware of these findings when reviewing or using MODIS data.

In the second chapter, I showed that significant differences can exist between MODIS collections. Therefore, in chapter 3, I evaluate the difference between MODIS and VIIRS, two separate but related sensors, as well as Landsat. I evaluate the consistency between MODIS and VIIRS because VIIRS is the designated successor to MODIS. It is pertinent to understand the

relationship between MODIS and VIIRS due to the degradation experienced by MODIS Terra. I find that there are prominent differences between the two, especially in forests. The correlation is stronger between datasets in grasslands, possibly due to the simplified structure of grasslands in comparison to forests.

Overall, this document suggests that the research community cannot naively assume the consistency of data sources. Although there is a great effort in creating consistent and accurate data products, the datasets should continue to be critically examined if sensors are used in conjunction or, in the case of MODIS, if a new collection has been rolled out. Additionally, in both chapters two and three, I show that land cover greatly impacts sensor agreement. Therefore, continued work needs be done on assessing how datasets perform across land covers, in complex landscapes. Only evaluating performance in quasi-stable calibration sites gives a limited perspective to how users can expect the data to perform.